ORIGINAL ARTICLE

Somatic Activating *KRAS* Mutations in Arteriovenous Malformations of the Brain

S.I. Nikolaev, S. Vetiska, X. Bonilla, E. Boudreau, S. Jauhiainen, B. Rezai Jahromi, N. Khyzha, P.V. DiStefano, S. Suutarinen, T.-R. Kiehl, V. Mendes Pereira, A.M. Herman, T. Krings, H. Andrade-Barazarte, T. Tung, T. Valiante, G. Zadeh, M. Tymianski, T. Rauramaa, S. Ylä-Herttuala, J.D. Wythe, S.E. Antonarakis, J. Frösen, J.E. Fish, and I. Radovanovic

ABSTRACT

BACKGROUND

Sporadic arteriovenous malformations of the brain, which are morphologically abnormal connections between arteries and veins in the brain vasculature, are a leading cause of hemorrhagic stroke in young adults and children. The genetic cause of this rare focal disorder is unknown.

METHODS

We analyzed tissue and blood samples from patients with arteriovenous malformations of the brain to detect somatic mutations. We performed exome DNA sequencing of tissue samples of arteriovenous malformations of the brain from 26 patients in the main study group and of paired blood samples from 17 of those patients. To confirm our findings, we performed droplet digital polymerase-chain-reaction (PCR) analysis of tissue samples from 39 patients in the main study group (21 with matching blood samples) and from 33 patients in an independent validation group. We interrogated the downstream signaling pathways, changes in gene expression, and cellular phenotype that were induced by activating *KRAS* mutations, which we had discovered in tissue samples.

RESULTS

We detected somatic activating *KRAS* mutations in tissue samples from 45 of the 72 patients and in none of the 21 paired blood samples. In endothelial cell–enriched cultures derived from arteriovenous malformations of the brain, we detected *KRAS* mutations and observed that expression of mutant KRAS ($KRAS^{G12V}$) in endothelial cells in vitro induced increased ERK (extracellular signal-regulated kinase) activity, increased expression of genes related to angiogenesis and Notch signaling, and enhanced migratory behavior. These processes were reversed by inhibition of MAPK (mitogen-activated protein kinase)–ERK signaling.

CONCLUSIONS

We identified activating *KRAS* mutations in the majority of tissue samples of arteriovenous malformations of the brain that we analyzed. We propose that these malformations develop as a result of KRAS-induced activation of the MAPK–ERK signaling pathway in brain endothelial cells. (Funded by the Swiss Cancer League and others.)

The authors' full names, academic degrees, and affiliations are listed in the Appendix. Address reprint requests to Dr. Nikolaev at sergey.nikolaev@unige.ch, to Dr. Frösen at juhana.frosen@kuh.fi, to Dr. Fish at jason.fish@utoronto.ca, or to Dr. Radovanovic at ivan.radovanovic@uhn.ca.

Drs. Nikolaev, Vetiska, Frösen, Fish, and Radovanovic contributed equally to this article.

This article was published on January 3, 2018, at NEJM.org.

DOI: 10.1056/NEJMoa1709449

Arteriovenous malformations of the brain are high-flow vascular malformations that occur in approximately 15 per 100,000 persons and cause hemorrhagic stroke in children.[1-4] They are tortuous, morphologically abnormal vascular channels between arteries and veins that lack an intervening capillary network, allowing high-pressure arterial blood from feeding arteries to shunt directly into the venous outflow system. The underlying cause of sporadic arteriovenous malformations of the brain is unknown, but similar lesions are found in rare genetic syndromes, such as hereditary hemorrhagic telangiectasias (a group of disorders caused by inactivating germline mutations in regulators of the transforming growth factor β–SMAD pathway[5-7]), and in the capillary malformation–arteriovenous malformation syndrome (a RASopathy that is caused by inactivating mutations of *RASA1* or *EPHB4*[8,9]). This pattern indicates that a genetic cause may underlie the development of arteriovenous malformations of the brain, but most of these malformations occur as sporadic lesions in persons without a family history of the disease. We hypothesized that arteriovenous malformations of the brain arise from somatic mutations in the cranial vasculature.

METHODS

STUDY PATIENTS

Patients were eligible for inclusion in the study if they had sporadic, unifocal arteriovenous malformations of the brain with a defined nidus and evidence of arteriovenous shunting on digital subtraction angiography. In addition, patients had to have no family history of arteriovenous malformations and no documented history of genetic vascular disease. Clinical and surgical information was obtained from patients' charts by the authorized study team. All diagnoses of arteriovenous malformations of the brain were confirmed by the study pathologists, radiologists, and surgeons (see Supplementary Appendix 1, available with the full text of this article at NEJM.org). All the patients, who were 18 years of age or older, provided written informed consent.

STUDY PROCEDURES, OUTCOMES, AND OVERSIGHT

The main study group comprised patients from Canada. Tissue samples of arteriovenous malformations of the brain and blood samples were obtained from these patients and deidentified, flash-frozen, and stored at Toronto Western Hospital, University Health Network, Toronto. Whole-exome sequencing was performed to detect somatic mutations. The results of DNA sequencing were confirmed with the use of droplet digital polymerase-chain-reaction (PCR) analysis. All the procedures performed with the use of samples obtained from patients were approved by the Institutional Research Ethics Review Board of the University Health Network. Details about the immunohistochemical analyses of the tissue samples are provided in Supplementary Appendix 1.

The independent validation group comprised patients from Finland. DNA samples were obtained from formalin-fixed, paraffin-embedded tissues of arteriovenous malformations of the brain from these patients. The samples were treated with a DNA glycosylase to reduce the risk of false positives on droplet digital PCR analysis, as described by Do and Dobrovic.[10] Droplet digital PCR analysis was performed to detect *KRAS* mutations. All the procedures performed with the use of samples obtained from patients were approved by the Research Ethics Board at the University of Eastern Finland. Additional information regarding the tissue samples that were obtained from the patients is provided in Supplementary Appendix 1.

CELLULAR AND MOLECULAR STUDIES

Freshly resected tissue samples of arteriovenous malformations of the brain or control samples of normal tissue from temporal lobectomy specimens were obtained for the main study group from Toronto Western Hospital. Endothelial-cell cultures were established according to a modification of methods that had been described previously[11] and were enriched and depleted with the use of anti-CD31 magnetic beads. Cell cultures were isolated from freshly resected tissue. Frozen tissues were used for exome sequencing and digital droplet PCR assays. The cell cultures were used for the digital droplet PCR assays and Western blotting. Details about the cellular and molecular studies to model mutant KRAS expression in cultured human cells are provided in Supplementary Appendix 1.

STATISTICAL ANALYSIS

Pairwise comparisons were made with the use of Student's *t*-test. Comparison of three or more groups was performed with the use of a one-way analysis of variance with the Newman–Keuls

post hoc test. A P value of 0.05 or less was considered to indicate statistical significance. The Q value is the adjusted P value that is found by means of an optimized false discovery rate approach, and the r value is the linear correlation coefficient.

RESULTS

PATIENTS

From January 2013 through October 2017, a total of 39 patients were included in the main study group and had samples of arteriovenous malformation stored in the neurosurgical tissue bank. Of those, 21 had matched blood samples and 6 had fresh arteriovenous-malformation tissue that was used to derive cell culture. In addition, fresh vessel samples that had been obtained from 3 patients undergoing temporal-lobe resection for epilepsy were included. Tissues from 2 patients with cavernous malformations and 1 with dural arteriovenous fistula as well as 2 samples of normal cortical vessels and 1 sample of gliosis tissue were included as controls. In the Finnish validation group, archived paraffin-embedded samples that had been obtained from 33 patients with arteriovenous malformations of the brain were included; 54 samples of arteries from the circle of Willis, 18 samples of cavernous malformations, and 2 samples of dural arteriovenous fistulas were also obtained for the control group.

DETECTION OF SOMATIC ACTIVATING *KRAS* MUTATIONS

In the main study group, whole-exome sequencing was performed on tissue samples of arteriovenous malformations of the brain that were obtained from 26 patients. Using the default criteria of MuTect2 variant caller, we detected six somatic missense variants in three genes, including two variants of unknown clinical significance (one in *PCSK5* and the other in *TP53BP1*) (see the Supplemental Methods Section in Supplementary Appendix 1). The other four identified variants mapped to the same genomic coordinate in *KRAS* (chr12:25398284), which corresponded to a c.35G→A (p.Gly12Asp) mutation (in Patients 1, 4, and 10) or a c.35G→T (p.Gly12Val) mutation (in Patient 2). These variants were present in 2.4 to 4.0% of the sequence reads per sample (mean sequence coverage, 339±64×). On analysis of the 17 paired blood samples, the exomes had good coverage for this site (mean sequence coverage, 121±41×); no sequence reads contained a variant (Fig. 1). On further analysis that was performed with the use of relaxed criteria (the presence of variants in >0.5% of sequence reads, with reads on both DNA strands; see the Supplemental Methods Section in Supplementary Appendix 1), *KRAS* mutations were present in tissue samples obtained from 12 of the 26 patients and in none of the 17 paired blood samples (Fig. 1). *KRAS* mutations were present in 0.9 to 4.1% of the sequence reads. Activating *KRAS* mutations were found at codon 12: the c.35G→T (p.Gly12Val) mutation was found in 4 patients and the c.35G→A (p.Gly12Asp) mutation in 8 patients, including 1 patient (Patient 1) in whom the nidus sample and the draining-vein sample contained the c.35G→A (p.Gly12Asp) mutation in 2.0% and 1.3% of the sequence reads, respectively. These mutations are known to confer constitutive activity on KRAS.[12] (Details of the analyses are shown in Table S1 in Supplementary Appendix 2 and Tables S2 and S3 and Fig. S1 in Supplementary Appendix 1.)

CONFIRMATION OF *KRAS* MUTATIONS

To confirm the results of whole-exome sequencing and to detect additional *KRAS* variants that may have been missed because of low representation in the sample, we performed droplet digital PCR analysis of the tissue samples obtained from the 26 patients (primer sequences are shown in Table S4 in Supplementary Appendix 1). We detected 12 putative *KRAS* mutations that had been detected previously on whole-exome sequencing and 6 *KRAS* mutations in previously negative samples (Fig. 1). We also tested 13 additional tissue samples, 4 of which had matching blood samples, with the use of droplet digital PCR analysis only; we detected the c.35G→A (p.Gly12Asp) mutation in 9 of these samples and the c.35G→T (p.Gly12Val) mutation in 2 of them (Fig. 1). The other 2 samples were nonmutated. Altogether, droplet digital PCR analysis revealed *KRAS* mutations in tissue samples from 29 of the 39 patients: 19 samples had the c.35G→A (p.Gly12Asp) mutation, 9 had the c.35G→T (p.Gly12Val) mutation, and 1 had the c.183A→T (p.Gln61His) mutation. The fractional abundance of variants in the unpurified tissue samples ranged from 0.43 to 4.37% (Fig. 1), a finding consistent with the results of whole-exome sequencing (r=0.72). The 21 paired blood samples were negative for *KRAS* mutations (fractional abundance, 0%; positive

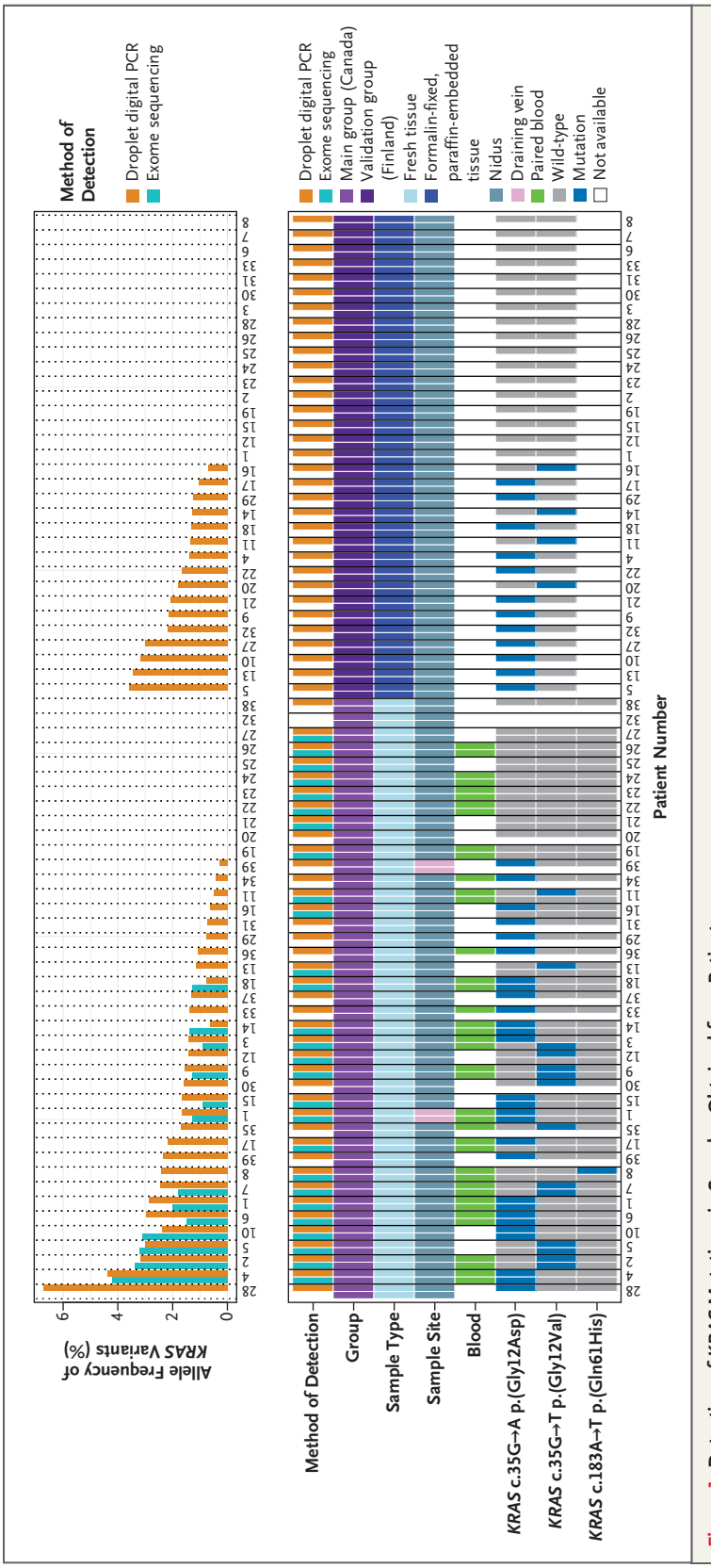

Figure 1. Detection of *KRAS* Mutations in Samples Obtained from Patients.

The top chart shows the allele frequency of *KRAS* variants, determined by either the percentage of sequence reads that contained variants on whole-exome sequencing or the fractional abundance of variants on digital droplet polymerase-chain-reaction (PCR) analysis, in tissue samples of arteriovenous malformations of the brain. The samples are shown according to patient number in order of highest to lowest frequency, first in the main study group, which included 39 patients from Canada (29 [74%] with *KRAS* mutations), and then in the independent validation group, which included 33 patients from Finland (16 [48%] with *KRAS* mutations). The bottom chart shows details about the samples, including the sample type (fresh-frozen or formalin-fixed, paraffin-embedded tissue), sample site (nidus or draining vein), the presence or absence of a paired blood sample, and the specific activating mutation detected. No *KRAS* mutations were detected in paired blood samples. The CD31+ cells from Patient 32 in the main study group were positive for a c.35G→A *KRAS* mutation (data not shown in this figure), but there was insufficient tissue remaining for whole tissue analysis. Two patients from the main study group (Patients 1 and 39) had *KRAS* mutations in the draining-vein sample that matched those observed in the nidus sample.

droplets, 0). Moreover, droplet digital PCR analysis of 3 samples from patients with vascular lesions of the brain that were not arteriovenous malformations (2 of cavernous malformations of the brain and 1 of a draining vein of a spinal dural arteriovenous fistula), 2 samples of normal cortical vessels, and 1 sample of gliosis tissue surrounding a cavernous malformation were negative for *KRAS* variants (fractional abundance, 0%; positive droplets, 0). (Details of the analyses are shown in Fig. S2 and in Tables S3 and S6 in Supplementary Appendix 1 and Table S5 in Supplementary Appendix 2.)

DETECTION OF *KRAS* MUTATIONS IN AN INDEPENDENT VALIDATION GROUP

The results in the main study group were validated in an independent validation group that involved 33 Finnish patients who had arteriovenous malformations of the brain. Genomic DNA was extracted from formalin-fixed, paraffin-embedded blocks of surgically resected tissue samples of arteriovenous malformations of the brain, and the DNA was analyzed with the use of droplet digital PCR analysis for the c.35G→A (p.Gly12Asp) and c.35G→T (p.Gly12Val) mutations in *KRAS*. To evaluate the level of sequence artifacts for these variants in DNA isolated from formalin-fixed, paraffin-embedded tissue,[10] we analyzed formalin-fixed, paraffin-embedded tissue samples from normal intracranial arteries and from vascular lesions of the brain that were not arteriovenous malformations: 54 samples of cadaveric brain arteries from the circle of Willis, 18 samples of cavernous malformations, and 2 samples of dural arteriovenous fistulas. The false positives in these samples did not exceed a fractional abundance of 0.52% for the c.35G→A (p.Gly12Asp) mutation and 0.14% for the c.35G→T (p.Gly12Val) mutation (mean fractional abundance, 0.25±0.10%). Taking this into account, we selected a threshold for fractional abundance of 1.00% for the c.35G→A (p.Gly12Asp) mutation and 0.50% for the c.35G→T (p.Gly12Val) mutation, with a requirement of at least 5 positive droplets for either variant.

Droplet digital PCR analysis of 33 tissue samples showed that the fractional abundance of *KRAS* variants exceeded the thresholds in 16 samples (48%). In findings that were similar to the results in the main study group, the fractional abundance of *KRAS* variants was low in the independent validation group (0.70 to 3.60%) (Fig. 1).

In formalin-fixed, paraffin-embedded tissue samples, false positives on droplet digital PCR analysis for the c.35G→A (p.Gly12Asp) mutation can result from deamination of cytosine to uracil. To reduce the risk of false positives, all the tissue samples that had been positive for the c.35G→A (p.Gly12Asp) mutation in *KRAS* and some samples of arteries from the circle of Willis were treated with uracil DNA glycosylase. We observed a reduction in fractional abundance in the samples of arteries from the circle of Willis but no reduction in the samples of brain arteriovenous-malformation tissue that had been positive for the *KRAS* variant. In addition to paraffin-embedded tissue, fresh-frozen tissue samples of arteriovenous malformations of the brain were available in three patients in the independent validation group (Patients 2, 3, and 10). The droplet digital PCR results that were obtained from fresh-frozen tissue samples were similar to the results that were obtained with the use of paraffin-embedded tissue obtained from the same patients. (Details of the analyses are shown in Fig. S3 and in Tables S3 and S8 in Supplementary Appendix 1 and Table S7 in Supplementary Appendix 2.)

DETECTION OF *KRAS* MUTATIONS IN ENDOTHELIAL CELLS

To identify the types of cells that have *KRAS* mutations in arteriovenous malformations of the brain, we used magnetic-activated cell sorting to enrich and deplete endothelial cells from six fresh cell cultures derived from arteriovenous malformations of the brain (from Patients 29, 30, 31, 32, 38, and 39) and to enrich and deplete endothelial cells from three control cultures of normal vascular cells derived from cortical vessels (from three different patients undergoing temporal lobectomy for epilepsy). The endothelial-cell–enriched fractions of the cultures were, as expected, enriched with CD31+ cells (CD31 is an endothelial marker) (Fig. 2A); however, these fractions retained some cells that expressed alpha smooth-muscle actin (α-SMA). In contrast, the endothelial-cell–depleted fractions did not have cells that expressed CD31 and were highly enriched with α-SMA+ cells (Fig. 2A). Droplet digital PCR analysis showed that the CD31+ cultures derived from five of the six samples obtained from patients were positive for the c.35G→A (p.Gly12Asp) or c.35G→T (p.Gly12Val) mutation in *KRAS*. Those cultures also had a

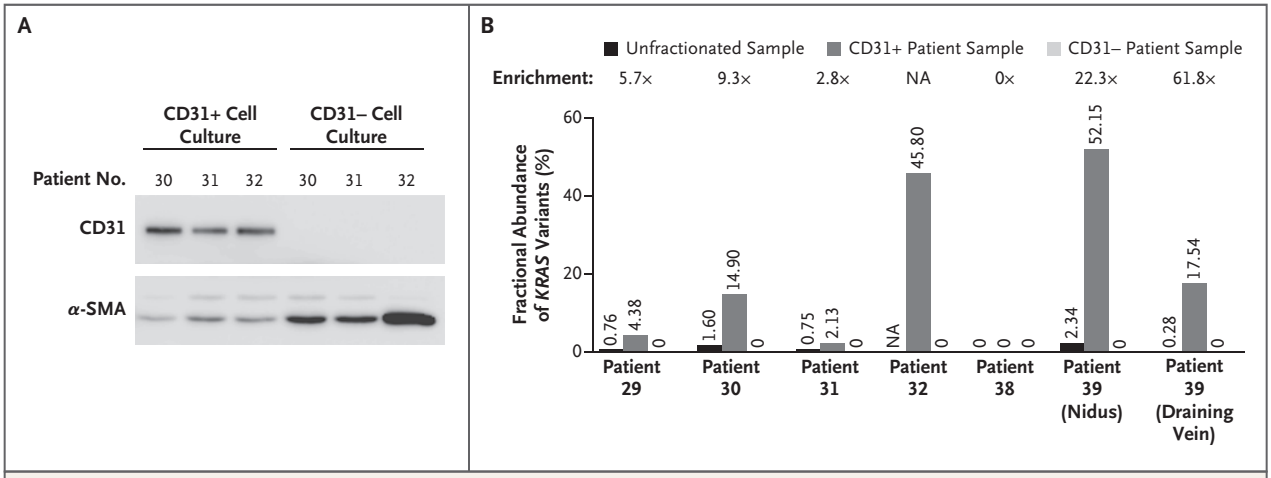

Figure 2. Detection of *KRAS* Mutations in Endothelial-Cell–Enriched and Endothelial-Cell–Depleted Cultures.

Panel A shows the expression of CD31 and alpha smooth-muscle actin (α-SMA) in endothelial-cell–enriched (CD31+) and endothelial-cell–depleted (CD31–) fractions of cell cultures derived from tissue samples of arteriovenous malformations of the brain that were obtained from patients. The CD31+ fractions (isolated with anti-CD31 magnetic beads) were composed of CD31+ cells and some α-SMA+ cells, whereas the CD31– fractions were devoid of CD31+ cells but contained α-SMA+ cells. Panel B shows the fractional abundance of *KRAS* variants in CD31+ and CD31– cell cultures derived from tissue samples of arteriovenous malformations of the brain and in the whole tissue sample before fractionation. Enrichment is the factor change of the fractional abundance in the CD31+ cells as compared with the whole unfractionated sample. The samples are from patients in the main study group. For Patient 32, all available tissue was used for cell culture and no tissue was left for digital droplet polymerase-chain-reaction analysis. NA denotes not available.

fractional abundance of variants that was 2.8 to 61.8 times as high as the level in whole tissue before fractionation, reaching 14.90% in Patient 30, 45.80% in Patient 32 (for whom whole unfractionated tissue was not available owing to the small amount of initial material), and 52.15% and 17.54% in the nidus and draining-vein samples, respectively, from Patient 39 (Fig. 2B).

In some samples, the fractional abundance of variants in the CD31+ cultures correlated with the percentage of CD31+ cells seen on immunostaining of low-passage (passage 1 to 2) CD31+ cultures: the nidus sample from Patient 32 (fractional abundance, 45.80% [i.e., >90% mutant *KRAS* cells]) had 87% CD31+ cells, and the draining-vein sample from Patient 39 (fractional abundance, 17.54% [i.e., >30% mutant *KRAS* cells]) had 30% CD31+ cells. These findings suggest that most endothelial cells derived from these samples were positive for *KRAS* mutations. In contrast, the CD31– cultures from the same samples were negative for *KRAS* mutations (Fig. 2B). Droplet digital PCR analysis of the control cell cultures did not reveal *KRAS* mutations in CD31+ or CD31– fractions. (Details of the analyses are shown in Figs. S2 and S4 and in Table S9 in Supplementary Appendix 1.)

ERK1/2 ACTIVATION IN ENDOTHELIAL CELLS WITH *KRAS* MUTATIONS

KRAS is an effector molecule that lies downstream of receptor tyrosine kinases, and it activates diverse cellular signaling networks, such as the RAF–MEK (mitogen-activated protein kinase [MAPK] kinase)–ERK (extracellular signal-regulated kinase) (MAPK–ERK) signaling pathway and the PI3K (phosphoinositide 3 kinase)–AKT–mTOR (mechanistic target of rapamycin) pathway.[12] We tested for phosphorylation of ERK1/2, AKT, and a noncanonical KRAS target, p38 MAPK,[13] in endothelial cell–enriched cultures derived from arteriovenous malformations of the brain with *KRAS* mutations and in human umbilical-vein endothelial cells (HUVECs) that expressed one of two isoforms (proteins encoded by differently spliced messenger RNA) of mutant $KRAS^{G12V}$: $KRAS4A^{G12V}$ or $KRAS4B^{G12V}$. The results for these cell cultures were compared with the results for primary endothelial cell–enriched cultures derived from normal brain vessels or HUVECs that received an empty expression construct. In both experiments, we observed increased levels of ERK1/2 phosphorylation in cells expressing mutant KRAS (Fig. 3A, and Fig. S5 in Supplementary Appendix 1) but did not observe increased

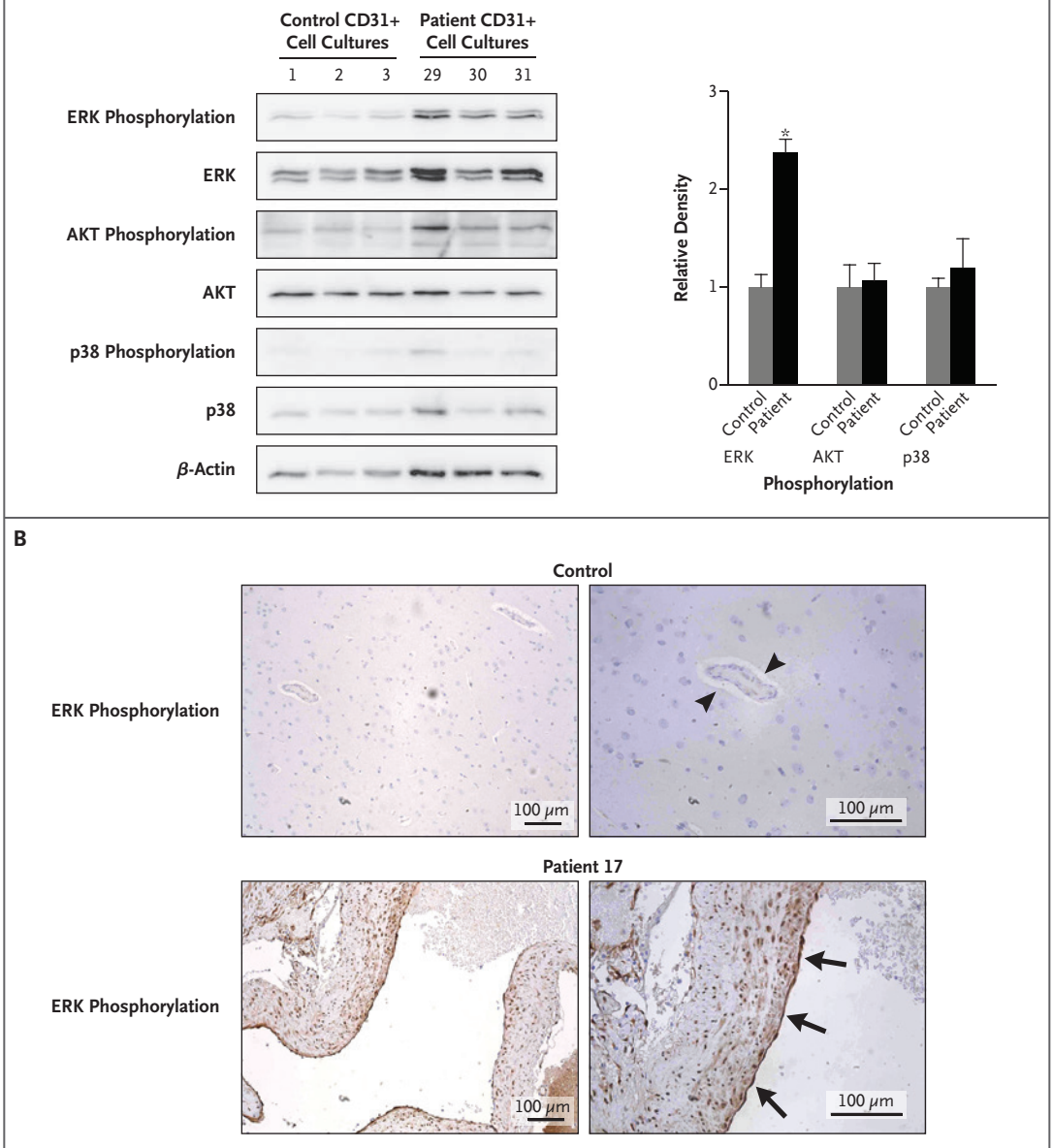

Figure 3. Detection of ERK Phosphorylation in Endothelial-Cell–Enriched Cell Cultures and Tissue Samples.

In Panel A, endothelial-cell–enriched (CD31+) cell cultures derived from tissue samples of arteriovenous malformations of the brain with *KRAS* mutations (from Patients 29, 30, and 31 in the main study group) show increased phosphorylation of ERK1/2 (extracellular signal-regulated kinase 1 or 2) but not of p38 or AKT, whereas three control CD31+ cell cultures derived from normal brain vasculature do not show increased phosphorylation of ERK1/2. Densitometry is shown on the right, normalized to beta-actin. The asterisk indicates a P value of 0.002. In Panel B, immunohistochemical staining of a tissue sample of an arteriovenous malformation of the brain with a *KRAS* mutation (from Patient 17 in the main study group) shows strong staining for ERK phosphorylation in endothelial cells lining the vascular lumen (arrows) and in vascular smooth-muscle cells in the vessel wall, whereas normal brain parenchymal vessels show little or no staining for ERK phosphorylation in endothelial cells (arrowheads).

levels of AKT or p38 phosphorylation. These findings suggest that mutant KRAS specifically activates the MAPK–ERK pathway in endothelial cells. Moreover, immunohistochemical staining of 25 tissue samples of arteriovenous malformations of the brain that were obtained from pa-

tients with arteriovenous malformations in the main study group and of 3 control samples of normal brain tissues was performed. There was strong staining for ERK phosphorylation in endothelial cells in the samples obtained from patients, regardless of the presence of a *KRAS* mutation, and little or no staining for ERK phosphorylation in the control samples (Fig. 3B).

PHENOTYPE OF ENDOTHELIAL CELLS WITH *KRAS* MUTATIONS

We performed RNA sequencing of HUVECs that expressed KRAS4A^{G12V}, KRAS4B^{G12V}, or control plasmid under growth factor–starved and serum-starved conditions. Assessment of categories of gene ontology that were altered in endothelial cells with KRAS^{G12V} expression revealed an enrichment of genes involved in the categories of angiogenesis or vascular development, proliferation, and migration. We also observed up-regulation of genes in the Notch pathway (e.g., *DLL4*, *JAG1*, *JAG2*, *NOTCH1*, *HES1*, and *HEY2*), which are involved in angiogenesis and arteriovenous specification[14,15] and have been implicated in the pathogenesis of arteriovenous malformations.[16] Arterial specification markers (e.g., *NRP1* and *EFNB2*) and venous specification markers (e.g., *EPHB4* and *NR2F2*) were unchanged. The expression of genes that are known to have a role in angiogenesis (e.g., *VEGFA*, *VEGFC*, *DUSP5*, and *HLX*) was also induced, as was the expression of genes that are characteristic of the endothelial-to-mesenchymal transition (e.g., *SNAI1*, *SNAI2*, *ZEB1*, and *PCDH1*), a process implicated in other vascular malformations.[17] These results imply that active KRAS dysregulates angiogenesis and vascular remodeling in endothelial cells. (For details, see Fig. S6 in Supplementary Appendix 1.)

Videos showing endothelial cells after KRAS activation are available at NEJM.org

The angiogenic factors vascular endothelial growth factor (VEGF) and fibroblast growth factor (FGF) activate intracellular signaling in a RAS-dependent manner.[18,19] Gene set enrichment analysis to compare the dysregulated genes in HUVECs that express KRAS^{G12V} with those in HUVECs that have been stimulated with VEGF[20] showed a robust correlation (normalized enrichment score, 2.01; Q<0.0001 for false discovery rate) (Fig. S6D in Supplementary Appendix 1). This finding suggests that, in the absence of exogenous stimulation, HUVECs that express KRAS^{G12V} behave like angiogenic endothelial cells.

HUVECs with KRAS4A^{G12V} expression had a highly elongated, mesenchymal-like phenotype (Fig. S7A in Supplementary Appendix 1). Time-lapse confocal imaging revealed that HUVECs that expressed KRAS4A^{G12V} were more migratory than control cells on a scratch-wound assay performed in the absence of exogenous angiogenic factors and appeared to have more rapid rearrangements of actin during migration, as assessed by live imaging of actin dynamics with the use of LifeAct-GFP (Video 1, available at NEJM.org, and Fig. S7A and S7B in Supplementary Appendix 1). In contrast to control cells, HUVECs that expressed KRAS4A^{G12V} were large and elongated and had rapid actin dynamics. F-actin was concentrated in lamellipodia on the periphery of the cells or moved in wavelike patterns through the cells. The cells were highly motile, even in the absence of a migratory signal (Fig. 4A and Video 2). Cell proliferation and apoptosis were unchanged in HUVECs that expressed KRAS4A^{G12V} (Fig. S7C and S7D in Supplementary Appendix 1). A phenotype with similar morphologic features, migratory patterns, and actin dynamics was seen in human aortic cells that had been transfected with KRAS4A^{G12V} (Video 3, and Fig. S8 in Supplementary Appendix 1).

Since cells that expressed KRAS4A^{G12V} did not form typical cobblestone monolayers (Fig.

Figure 4. Phenotype of Endothelial Cells Expressing Active KRAS.

Panel A shows time-lapse confocal images of human umbilical-vein endothelial cells (HUVECs) with KRAS4A^{G12V} expression and control cells. In the absence of exogenous angiogenic factors or a migratory cue (e.g., scratch wound), KRAS4A^{G12V} expression altered the actin dynamics (assessed by cotransfected LifeAct-GFP), including a reduction in the number of filopodia and an increase in lamellipodia formation (lamellipodia are indicated by arrows). Actin turnover was more rapid, and cells had increased motility; the images obtained at 80 minutes and 160 minutes show a gray outline of the position of the cells at 0 minutes. Panel B shows staining for vascular endothelial cadherin, ERK phosphorylation, and F-actin (assessed by cotransfected LifeAct-GFP) in HUVECs with KRAS4A^{G12V} expression, HUVECs with KRAS4A^{G12V} expression and MAPK–ERK inhibition with a MEK inhibitor for 16 hours, and control cells. KRAS4A^{G12V} activated the MAPK–ERK pathway and promoted disassembly of adherens junctions. MAPK–ERK inhibition re-established the formation of adherens junctions and normalized actin localization (arrows) and cell shape. Panel C is a heat map showing the expression of vascular endothelial growth factor (VEGF)–regulated genes in HUVECs expressing KRAS4A^{G12V}, treated with vehicle, MEK inhibitor, or phosphoinositide 3 kinase (PI3K) inhibitor for 6 hours in serum-starvation media. Data were compared with control cells treated with vehicle.

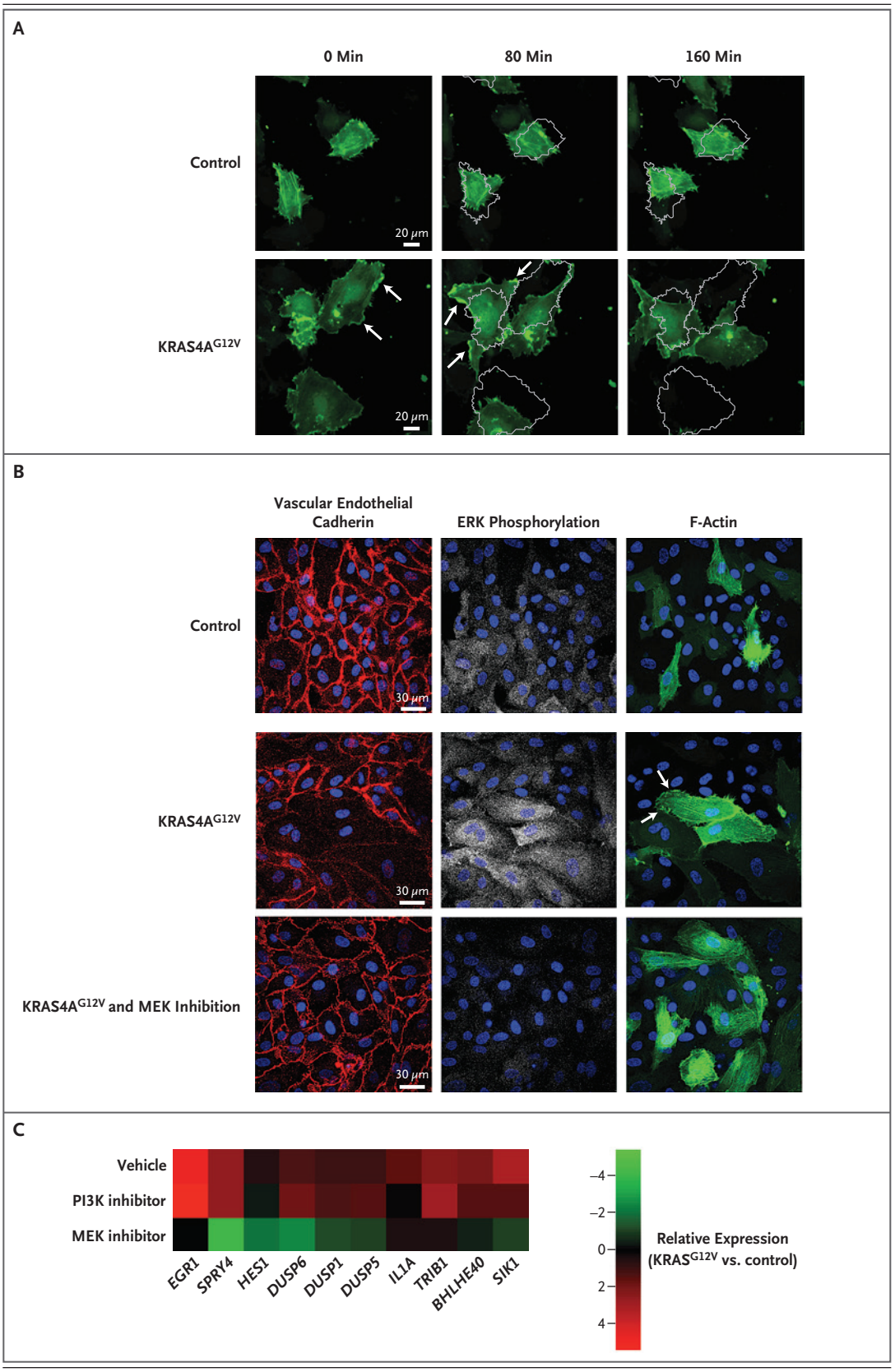

S7A in Supplementary Appendix 1), we assessed formation of adherens junctions. Expression of KRAS4A^{G12V} led to disassembly of vascular endothelial cadherin junctions (Fig. 4B). The inhibition of MAPK–ERK signaling with the use of a MEK inhibitor suppressed ERK phosphorylation, restored localization of vascular endothelial cadherin to the junctions of endothelial cells, and appeared to reduce lamellipodia formation (Fig. 4B). In addition, inhibition of the MAPK–ERK pathway abrogated the VEGF-like gene signature that was induced by KRAS4A^{G12V}, but inhibition of the PI3K pathway did not (Fig. 4C), a finding that reinforces the notion that the phenotype induced in endothelial cells by mutations that constitutively activate KRAS is specifically mediated by the MAPK–ERK pathway.

DISCUSSION

Somatic activating *KRAS* mutations were present in the majority of tissue samples of sporadic, nonfamilial arteriovenous malformations of the brain that we analyzed. They were accompanied by dysregulation of the MAPK–ERK pathway. This finding is consistent with the fact that other types of vascular malformation are caused by somatic mutations in genes in the PI3K or RAS–MAPK pathways. "Slow flow" vascular malformations are often associated with activating mutations in genes in the PI3K pathway,[21,22] whereas "high flow" vascular anomalies, including sporadic arteriovenous malformations of the brain, tend to be associated with activating mutations in genes in the RAS–MAPK pathway.[23-26]

The finding of relatively low allele frequencies of *KRAS* variants in sporadic arteriovenous malformations of the brain (0.5 to 4%) is consistent with the cellular heterogeneity of arteriovenous malformations[27] and the small fraction of endothelial cells therein and is consistent with the low frequencies of somatic mutations found in other genes in other types of vascular malformation (0.8 to 27%).[22,23,25,26] The detection of *KRAS* mutations in endothelial cell–enriched fractions from primary cultures but not in endothelial cell–depleted fractions from the same cultures suggests that *KRAS* mutations are probably specific to endothelial cells and that dysregulation of the biology of endothelial cells is a key feature of the formation of arteriovenous malformations of the brain. Moreover, the allele frequencies of the *KRAS* variants correlated with the percentages of endothelial cells in enriched fractions, which suggests that these variants are present in most endothelial cells isolated from arteriovenous malformations of the brain, arise early in the development of the malformations, and are probably primary events in the pathogenesis of the malformations.

How might alterations in RAS signaling in endothelial cells induce arteriovenous malformations? The mutations that we have identified are known to drive strong and constitutive MAPK–ERK signaling[28] and are important drivers of tumorigenesis.[29] Arteriovenous malformations of the brain are not associated with cancer, which suggests a context-dependent role for *KRAS* mutations in the endothelium. The finding that somatic activating *KRAS* mutations in endometriosis do not cause cancer is consistent with this interpretation.[30]

Our initial in vitro exploration of endothelial-cell phenotypes after KRAS activation showed increased expression of angiogenic genes such as *VEGFA*/*C* and genes encoding proteins in the Notch signaling pathway. These transcriptional changes are accompanied by a cellular phenotype that includes enhanced migratory behavior and disassembly of adherens junctions. Previous studies have shown that increased VEGF and Notch signaling are relevant to the development and maintenance of arteriovenous malformations of the brain.[31-37] Some of the in vitro phenotypes that we observed could be reverted to normal by means of inhibition of MAPK–ERK signaling. Our finding of increased MAPK–ERK signaling in endothelial cells from arteriovenous malformations of the brain without a *KRAS* variant suggests that activation of the MAPK–ERK pathway may be a defining feature of arteriovenous malformations of the brain. In the absence of available direct pharmacologic inhibitors of KRAS, small-molecule MEK inhibitors, which are used in clinical practice for treating cancers,[38] represent candidates for testing in clinical trials to treat arteriovenous malformations of the brain.

Supported by research grants to Dr. Nikolaev from the Swiss Cancer League (LSCC 2939-02-2012 and KSF-3985-08-2016), Dinu Lipatti (2014), and Novartis (14B065). Ms. Khyzha was supported by a Canada Graduate Scholarship from the Natural Sciences and Research Council of Canada. Dr. DiStefano was supported by a Postdoctoral Fellowship from the Toronto General Hospital Research Institute. Dr. Suutarinen was supported by a research grant from the Petri Honkanen Foundation. Dr. Herman was supported by a grant from the National Institutes of Health (2T32HL007676). Dr. Wythe was supported by an American Heart Association Grant-in-Aid (16GRNT31330023). Dr. Antonarakis was supported by a grant from the European Research Coun-

cil. Dr. Frösen was supported by research grants from the Finnish Medical Foundation and Kuopio University Hospital. Dr. Fish was supported by an operating grant from the Canadian Institutes of Health Research (CIHR) (MOP-119506) and a Team Project Award from the University of Toronto Medicine by Design initiative, which receives funding from the Canada First Research Excellence Fund and a Canada Foundation for Innovation equipment grant; he also received an Early Researcher Award from the Ontario Ministry of Research and Innovation and funding from the Canada Research Chair Program from the CIHR. Dr. Radovanovic was supported by the Timothy P. Susco Chair of Research Award from the Brain Aneurysm Foundation, the Toronto General and Western Hospital Foundation, and received seed support from the Department of Surgery and Division of Neurosurgery at the University Health Network.

Disclosure forms provided by the authors are available with the full text of this article at NEJM.org.

We thank the staff of the Princess Margaret Genomics Centre and Bioinformatics Services (C. Virtanen and Z. Lu) for generating the RNA and DNA sequencing data used in this study; the staff of the Centre for Applied Genomics at the Toronto Hospital for Sick Children (T. Paton) for performing droplet digital polymerase-chain-reaction analyses; Zhiqi Chen from University Health Network for help with cell biology assays; and Melanie Peralta from the Pathology Research Program, University Health Network, Toronto, for technical help with immunohistochemical analyses.

APPENDIX

The authors' full names and academic degrees are as follows: Sergey I. Nikolaev, Ph.D., Sandra Vetiska, Ph.D., Ximena Bonilla, M.D., Ph.D., Emilie Boudreau, M.Sc., Suvi Jauhiainen, Ph.D., Behnam Rezai Jahromi, M.B., Nadiya Khyzha, B.Sc., Peter V. DiStefano, Ph.D., Santeri Suutarinen, M.B., Tim-Rasmus Kiehl, M.D., Vitor Mendes Pereira, M.D., Alexander M. Herman, Ph.D., Timo Krings, M.D., Hugo Andrade-Barazarte, M.D., Ph.D., Takyee Tung, B.Sc., Taufik Valiante, M.D., Ph.D., Gelareh Zadeh, M.D., Ph.D., Mike Tymianski, M.D., Ph.D., Tuomas Rauramaa, M.D., Ph.D., Seppo Ylä-Herttuala, M.D., Ph.D., Joshua D. Wythe, Ph.D., Stylianos E. Antonarakis, M.D., Ph.D., Juhana Frösen, M.D., Ph.D., Jason E. Fish, Ph.D., and Ivan Radovanovic, M.D., Ph.D.

The authors' affiliations are as follows: the Department of Genetic Medicine and Development, University of Geneva Medical School (S.I.N., X.B., S.E.A.), Service of Genetic Medicine, University Hospitals of Geneva (S.I.N., S.E.A.), and iGE3, Institute of Genetics and Genomics of Geneva (S.E.A.) — all in Geneva; the Department of Fundamental Neurobiology, Krembil Research Institute (S.V., M.T., I.R.), Toronto General Hospital Research Institute (E.B., N.K., P.V.D., J.E.F.), the Department of Pathology (T.-R.K.), the Division of Neurosurgery, Department of Surgery (V.M.P., T.K., H.A.-B., T.T., T.V., G.Z., M.T., I.R.), and the Joint Division of Medical Imaging, Department of Medical Imaging (V.M.P., T.K.), Toronto Western Hospital, University Health Network, the Department of Laboratory Medicine and Pathobiology, University of Toronto (E.B., N.K., P.V.D., T.-R.K., J.E.F.), and the Heart and Stroke Richard Lewar Centre of Excellence in Cardiovascular Research (E.B., N.K., P.V.D., J.E.F.) — all in Toronto; the Department of Molecular Medicine, AIV Institute, University of Eastern Finland (S.J., B.R.J., S.S., S.Y.-H., J.F.), and the Hemorrhagic Brain Pathology Research Group, Department of Neurosurgery and NeuroCenter (S.J., B.R.J., S.S., T.R., J.F.), and the Department of Pathology (T.R.), Kuopio University Hospital — all in Kuopio, Finland; and the Cardiovascular Research Institute and the Department of Molecular Physiology and Biophysics, Baylor College of Medicine, Houston (A.M.H., J.D.W.).

REFERENCES

1. Brown RD Jr, Wiebers DO, Torner JC, O'Fallon WM. Incidence and prevalence of intracranial vascular malformations in Olmsted County, Minnesota, 1965 to 1992. Neurology 1996;46:949-52.

2. Berman MF, Sciacca RR, Pile-Spellman J, et al. The epidemiology of brain arteriovenous malformations. Neurosurgery 2000; 47:389-97.

3. Al-Shahi R, Warlow C. A systematic review of the frequency and prognosis of arteriovenous malformations of the brain in adults. Brain 2001;124:1900-26.

4. Al-Shahi R, Fang JS, Lewis SC, Warlow CP. Prevalence of adults with brain arteriovenous malformations: a community based study in Scotland using capture-recapture analysis. J Neurol Neurosurg Psychiatry 2002;73:547-51.

5. McAllister KA, Grogg KM, Johnson DW, et al. Endoglin, a TGF-beta binding protein of endothelial cells, is the gene for hereditary haemorrhagic telangiectasia type 1. Nat Genet 1994;8:345-51.

6. Johnson DW, Berg JN, Baldwin MA, et al. Mutations in the activin receptor-like kinase 1 gene in hereditary haemorrhagic telangiectasia type 2. Nat Genet 1996;13:189-95.

7. Gallione CJ, Repetto GM, Legius E, et al. A combined syndrome of juvenile polyposis and hereditary haemorrhagic telangiectasia associated with mutations in MADH4 (SMAD4). Lancet 2004;363:852-9.

8. Revencu N, Boon LM, Mulliken JB, et al. Parkes Weber syndrome, vein of Galen aneurysmal malformation, and other fast-flow vascular anomalies are caused by RASA1 mutations. Hum Mutat 2008;29: 959-65.

9. Amyere M, Revencu N, Helaers R, et al. Germline loss-of-function mutations in EPHB4 cause a second form of capillary malformation-arteriovenous malformation (CM-AVM2) deregulating RAS-MAPK signaling. Circulation 2017;136:1037-48.

10. Do H, Dobrovic A. Dramatic reduction of sequence artefacts from DNA isolated from formalin-fixed cancer biopsies by treatment with uracil-DNA glycosylase. Oncotarget 2012;3:546-58.

11. Boscolo E, Pavesi G, Zampieri P, et al. Endothelial cells from human cerebral aneurysm and arteriovenous malformation release ET-1 in response to vessel rupture. Int J Mol Med 2006;18:813-9.

12. Simanshu DK, Nissley DV, McCormick F. RAS proteins and their regulators in human disease. Cell 2017;170:17-33.

13. Cuadrado A, Nebreda AR. Mechanisms and functions of p38 MAPK signalling. Biochem J 2010;429:403-17.

14. Benedito R, Hellström M. Notch as a hub for signaling in angiogenesis. Exp Cell Res 2013;319:1281-8.

15. Fish JE, Wythe JD. The molecular regulation of arteriovenous specification and maintenance. Dev Dyn 2015;244:391-409.

16. ZhuGe Q, Zhong M, Zheng W, et al. Notch-1 signalling is activated in brain arteriovenous malformations in humans. Brain 2009;132:3231-41.

17. Maddaluno L, Rudini N, Cuttano R, et al. EndMT contributes to the onset and progression of cerebral cavernous malformations. Nature 2013;498:492-6.

18. Kouhara H, Hadari YR, Spivak-Kroizman T, et al. A lipid-anchored Grb2-binding protein that links FGF-receptor activation to the Ras/MAPK signaling pathway. Cell 1997;89:693-702.

19. Meadows KN, Bryant P, Pumiglia K. Vascular endothelial growth factor induction of the angiogenic phenotype requires Ras activation. J Biol Chem 2001;276: 49289-98.

20. Zhang B, Day DS, Ho JW, et al. A dynamic H3K27ac signature identifies VEGFA-stimulated endothelial enhancers and requires EP300 activity. Genome Res 2013; 23:917-27.

21. Limaye N, Wouters V, Uebelhoer M, et al. Somatic mutations in angiopoietin receptor gene TEK cause solitary and multiple sporadic venous malformations. Nat Genet 2009;41:118-24.

22. Limaye N, Kangas J, Mendola A, et al. Somatic activating PIK3CA mutations cause venous malformation. Am J Hum Genet 2015;97:914-21.

23. Couto JA, Vivero MP, Kozakewich HP, et al. A somatic MAP3K3 mutation is as-

sociated with verrucous venous malformation. Am J Hum Genet 2015;96:480-6.
24. Couto JA, Huang L, Vivero MP, et al. Endothelial cells from capillary malformations are enriched for somatic GNAQ mutations. Plast Reconstr Surg 2016;137(1):77e-82e.
25. Ayturk UM, Couto JA, Hann S, et al. Somatic activating mutations in GNAQ and GNA11 are associated with congenital hemangioma. Am J Hum Genet 2016;98:789-95.
26. Couto JA, Huang AY, Konczyk DJ, et al. Somatic MAP2K1 mutations are associated with extracranial arteriovenous malformation. Am J Hum Genet 2017;100:546-54.
27. Finby N, Begg CF. Arteriovenous malformation of the brain. N Y State J Med 1965;65:554-8.
28. Cagnol S, Rivard N. Oncogenic KRAS and BRAF activation of the MEK/ERK signaling pathway promotes expression of dual-specificity phosphatase 4 (DUSP4/MKP2) resulting in nuclear ERK1/2 inhibition. Oncogene 2013;32:564-76.
29. Park JT, Johnson N, Liu S, et al. Differential in vivo tumorigenicity of diverse KRAS mutations in vertebrate pancreas: a comprehensive survey. Oncogene 2015;34:2801-6.
30. Anglesio MS, Papadopoulos N, Ayhan A, et al. Cancer-associated mutations in endometriosis without cancer. N Engl J Med 2017;376:1835-48.
31. Uranishi R, Baev NI, Ng PY, Kim JH, Awad IA. Expression of endothelial cell angiogenesis receptors in human cerebrovascular malformations. Neurosurgery 2001;48:359-68.
32. Hashimoto T, Lawton MT, Wen G, et al. Gene microarray analysis of human brain arteriovenous malformations. Neurosurgery 2004;54:410-25.
33. Murphy PA, Lam MT, Wu X, et al. Endothelial Notch4 signaling induces hallmarks of brain arteriovenous malformations in mice. Proc Natl Acad Sci U S A 2008;105:10901-6.
34. Murphy PA, Lu G, Shiah S, Bollen AW, Wang RA. Endothelial Notch signaling is upregulated in human brain arteriovenous malformations and a mouse model of the disease. Lab Invest 2009;89:971-82.
35. Murphy PA, Kim TN, Lu G, Bollen AW, Schaffer CB, Wang RA. Notch4 normalization reduces blood vessel size in arteriovenous malformations. Sci Transl Med 2012;4:117ra8.
36. Murphy PA, Kim TN, Huang L, et al. Constitutively active Notch4 receptor elicits brain arteriovenous malformations through enlargement of capillary-like vessels. Proc Natl Acad Sci U S A 2014;111:18007-12.
37. Li S, Wang R, Wang Y, et al. Receptors of the Notch signaling pathway are associated with hemorrhage of brain arteriovenous malformations. Mol Med Rep 2014;9:2233-8.
38. Zhao Y, Adjei AA. The clinical development of MEK inhibitors. Nat Rev Clin Oncol 2014;11:385-400.

Supplementary Appendix 1

This appendix has been provided by the authors to give readers additional information about their work.

Supplement to: Nikolaev SI, Vetiska S, Bonilla X, et al. Somatic activating *KRAS* mutations in arteriovenous malformations of the brain. N Engl J Med 2018;378:250-61. DOI: 10.1056/NEJMoa1709449

Supplementary Appendix:

Somatic Activating *KRAS* Variants in Brain Arteriovenous Malformations

List of investigators:

Sergey I Nikolaev, Ph.D [1,2,†,*], Sandra Vetiska, Ph.D [3,†], Ximena Bonilla, M.D., Ph.D [1], Emilie Boudreau, M.Sc [4,5,6], Suvi Jauhiainen, Ph.D. [7,8], Behnam Rezai Jahromi, M.B. [7,8], Nadiya Khyzha, B.S. [4,5,6], Peter V. DiStefano, Ph.D. [4,5,6], Santeri Suutarinen, M.B. [7,8], Tim-Rasmus Kiehl, M.D. [5,9], Vitor Mendes Pereira, M.D. [10,11], Alexander M. Herman, Ph.D. [12,13], Timo Krings, M.D. [10, 11], Hugo Andrade-Barazarte, M.D., Ph.D [10], Takyee Tung, B.Sc. [10], Taufik Valiante, M.D., Ph.D. [10], Gelareh Zadeh, M.D., Ph.D. [10], Mike Tymianski, M.D., Ph.D. [3,10], Tuomas Rauramaa, M.D., Ph.D [8,14], Seppo Ylä-Herttuala, M.D., Ph.D. [7], Joshua D. Wythe, Ph.D. [12,13], Stylianos E. Antonarakis, M.D. [1,2,15], Juhana Frösen, M.D., Ph.D [8,*], Jason E. Fish, Ph.D.[4,5,6,§,*], Ivan Radovanovic, M.D. , Ph.D [3,10,§,*].

[1] Department of Genetic Medicine and Development, University of Geneva Medical School, Switzerland
[2] Service of Genetic Medicine, University Hospitals of Geneva, Switzerland
[3] Department of Fundamental Neurobiology, Krembil Research Institute, University Health Network, Toronto, Canada
[4] Toronto General Hospital Research Institute, University Health Network, Toronto, Canada
[5] Department of Laboratory Medicine & Pathology, University of Toronto, Canada
[6] Heart & Stroke Richard Lewar Centre of Excellence in Cardiovascular Research, Toronto, Canada
[7] Department of Molecular Medicine, AIV-Institute, University of Eastern Finland
[8] Hemorrhagic Brain Pathology Research Group, Department of Neurosurgery/NeuroCenter, Kuopio University Hospital and University of Eastern Finland
[9] Department of Pathology, University Health Network, Toronto, Canada
[10] Division of Neurosurgery, Department of Surgery, University Health Network, Toronto, Canada
[11] Joint Division of Medical Imaging, Department of Medical Imaging, Toronto Western Hospital, University Health Network, Toronto, Ontario, Canada
[12] Cardiovascular Research Institute, Baylor College of Medicine, Houston, Texas, USA
[13] Department of Molecular Physiology and Biophysics, Baylor College of Medicine, Houston, Texas, USA
[14] Department of Pathology, Kuopio University Hospital and University of Eastern Finland
[15] iGE3, Institute of Genetics and Genomics of Geneva, Switzerland

Table of Contents

Supplemental Methods **3**
Clinical diagnosis and treatment of BAVMs 3
Sample preparation and exome sequencing: 3
Digital Droplet PCR (ddPCR) - Toronto cohort: 5
DNA isolation and *KRAS* ddPCR from paraffin embedded and frozen samples in the Kuopio University Hospital replication cohort 6
Cell culture of AVM and normal brain vascular endothelial cells: 7
Cell culture and treatment of human umbilical vein endothelial cells (HUVECs) 8
Cell culture of telomerize-immortalized human aortic endothelial cells (TeloHAEC) 8
Plasmids: 8
Electroporation: 8
Transfection of TeloHAEC 9
Gene expression and cell biology experiments: 9
Confocal microscopy: 10
RNA isolation, and qRT-PCR 10
Immunofluorescence: 10
SDS-PAGE and Immunoblotting: 11
Immunohistochemistry: 11
RNA sequencing: 11
GSEA analysis 12
References 12

Supplemental Tables **14**
Table S1: Excel spreadsheet showing MuTec2 results for the 6 coding missense variants including 4 variants causing a *KRAS* c.35G>A;p.(Gly12Asp) mutation in 4 patients 14
Table S2: Summary of *KRAS* variants found with exome sequencing of the Toronto cohort using two algorithms, MuTecT2 and Variant Checker 14
Table S3: Summary of somatic variants of *KRAS* in brain arteriovenous malformation tissue samples from Toronto and Kuopio 15
Table S4: Primers used for ddPCR analyses 19
Table S5: Excel spreadsheet showing the number of positive events and the number of wild-type and total events for every Toronto BAVM sample tested by *KRAS* c.35G>T;p.(Gly12Val)- or c.35G>A;p.(Gly12Asp)-specific ddPCR [Included as a separate Excel file] 20
Table S6: Summary of clinical data and *KRAS* status of Fresh Frozen Toronto patients 20
Table S7: Excel spreadsheet showing the number of positive events and the number of wild-type events for every Kuopio sample tested by ddPCR, including UDC treatment of FFPE BAVM and control vascular samples [Included as a separate Excel file] 21
Table S8: Summary of clinical data and ddPCR results of Finnish FFPE BAVM samples 21
Table S9: ddPCR results and fractional abundance of *KRAS* variants in MAC-sorted $CD31^+$ and $CD31^-$ fractions of primary vascular cell cultures of BAVMs and normal brain vessels. 22
Table S10: Primers used for qRT-PCR analyses 23

Supplemental Methods

Clinical diagnosis and treatment of BAVMs

The clinical diagnosis of brain arteriovenous malformation for all patients included in this study was initially performed as standard clinical practice and was part of clinical care documented in the patient chart. Diagnosis was made at clinical presentation and before treatment by a multidisciplinary group consisting of surgeons, interventional neuroradiologists and neurosurgeons practicing or familiar with radiosurgery of AVMs. All patients were discussed formally in a multidisciplinary AVM conference and a consensus treatment decision was made (i.e. surgical resection of the BAVM). For the Toronto cohort, treatment (surgical resection) was done by IR and MT and based on the above mentioned diagnostic process after written informed consent for the treatment and for tissue storage and use for research purposes was obtained. After surgical resection, a staff neuropathologist confirmed the diagnosis as per standard clinical care protocol with a standard pathology report included as part of the patient chart. For the purpose of this study specifically, the diagnosis was re-reviewed and confirmed by IR and HAB (surgeons), VMP and TK (interventional neuroradiologists) and TRK (pathologist). Clinical data was collected by IR, HAB and VMP. For the Kuopio cohort, AVM diagnosis was confirmed by the treating radiologist, operating surgeon and neuropathologist. JFr reviewed the reports of all three and personally assessed the histopathology and the available imaging studies.

Sample preparation and exome sequencing:

Frozen BAVM samples and paired blood (leukocyte-enriched fraction) were obtained from the BAVM tissue bank at the Division of Neurosurgery at the University Health Network (UHN) in Toronto. All patients signed an informed consent agreement and the study was approved by the Research Ethics Board of UHN. BAVM samples were ground in liquid nitrogen using a mortar and pestle. Some of this ground tissue was used for DNA extraction and, when sufficient tissue was obtained, some was frozen for further experimental studies. Commercially available kits (e.g. QIAGEN Gentra Puregene) with established protocols were used to isolate genomic DNA for whole exome sequencing and downstream analyses.

Exome sequencing was performed by the Princess Margaret Genomics Centre, Toronto,

Canada, using a SureSelect V5 kit (Agilent). For library preparation, the Agilent SureSelect XT target enrichment kit was used with 200 ng of DNA from BAVMs or blood samples. Libraries were sequenced on an Illumina HiSeq2000 instrument with 100 bp paired-end sequencing, with a median coverage of 190x ± 43 for BAVMs and 80x ± 14 for blood samples. Average Illumina error rate for sequenced samples was 0.38 +/- 0.07% for read 1 and 0.4 +/- 0.09% for read 2, with a cluster density of ~930 K/mm^2. The mean of >= Q30 bases was 91.83%. Sequencing reads were mapped to the reference genome with the Burrows-Wheeler Aligner (BWA) [1] and then processed with the Genome Analysis Toolkit (GATK version 3.3.0) [2] following best practices for exome sequencing. Sequencing quality and target enrichment were verified with Picard tools metrics (http://broadinstitute.github.io/picard/). For the BAVMs with a matching germline sample, MuTect version 1.1.4 [3] with standard parameters was used to identify somatic single nucleotide variants (SNVs) and the GATK's HaplotypeCaller was used to call somatic insertions or deletions (e.g. "indels"). For the 9 samples for which a matched germline control sample was not available, a Panel of Normals (PON) was constructed from 50 germ-line samples. Functional variants including stop gain, splice site, or damaging (as predicted by PolyPhen2 [4]) and non-synonymous mutations were considered as putative drivers. Additionally, variants were considered putative drivers if they were reported in the COSMIC v76 database and were absent in ExAC Version 0.3 (or present with less than 0.00001 MAF). Due to high tissue heterogeneity of the BAVM tissue samples, the fraction of the cells with the causative mutation could be small, therefore the Variant Allele Frequency (VAF) of putative somatic variants is expected to be low. In order to detect candidate variants with low VAF we applied a multistep approach. Primarily, we analyzed 17 BAVMs for which a matching blood sample was available and selected somatic variants with the "KEEP" flag in the repeat masked target regions using MuTect2. Additionally, we screened for the candidate variants with the "REJECT" flag, which were rejected due to their VAF being <3% (default setting of MuTect2). Furthermore, we performed another high sensitivity and low specificity analysis on *KRAS* using a homemade algorithm, "VariantChecker", that screens all sites known to be recurrently mutated in cancer and reports VAF of non-reference nucleotides. This analysis reported all *KRAS* missense variants with a VAF >0.5% which were present on forward and reverse strand reads, or at least present in 5 reads on one strand (similar to [5]).

MuTect2 analysis of 17 BAVM–blood pairs rendered 22,351 variants. Of these variants, only 475 passed the internal MuTect2 quality filter (judgement==TRUE). All frequent variants, present in ExAC 0.3.1 database with a frequency more than 0.00002, were further filtered out, which reduced the number of candidate somatic functional variants to 164. Lastly, we applied stringent filtering criteria based on the coverage, VAFs, variant reads per strand, and quality of the predictions (Performed with the homemade tools (Variant Checker); Table S1):

1/ number of alternative reads in BAVM more than 6: "t_alt_count > 6";

2/ fraction of alternative reads in BAVM more than 2%: "tumor_f > 0.02";

3/ alternative reads on the forward strand should be present: "i_t_ALT_F1R2 > 0";

4/ alternative reads on the reverse strand should be present: "i_t_ALT_F2R1 > 0";

5/ alternative reads in the control sample should be absent: "n_alt_count == 0";

6/ the coverage in the control sample should be more than 60 fold: "n_ref_count + n_alt_count > 60";

7/ the coverage in the BAVM sample should be more than 150 fold "t_ref_count + t_alt_count >= 150";

8/ The tumor LOD score should be more than 10: "t_lod_fstar__INFO__ >10"

Application of such criteria resulted in a set of 9 SNVs which includes 6 missense variants; 4 *KRAS* variants at position chr12:25398284 and 2 in other genes (*TP53BP1* p.Leu55Phe, *PCSK5* p.Ala1783Val)

Digital Droplet PCR (ddPCR) - Toronto cohort:

Detection of rare variants in *KRAS* was performed on the QX200 Droplet Digital PCR system (Bio-Rad Laboratories, Inc., Hercules, CA, USA) at The Centre for Applied Genomics (TCAG) at The Hospital for Sick Children (Toronto, Canada) using Taqman hydrolysis probe chemistry (Life Technologies, Carlsbad, CA, USA). A 40X custom genotyping primer and probe mix was designed for each variant. The 20 μL reaction mix consisted of 10 μL of 2x ddPCR SuperMix for Probes (Bio-Rad Laboratories), 0.5 μL of the 40X SNP genotyping assay, 8.5 μL water and 1 μL of 50 ng/μL genomic DNA. Cycling conditions for the reaction were 95°C for 10 min, followed by 45 cycles of 94°C for 30 sec and 60°C for 1 min, then 98°C for 10 minutes, and finally a 10°C hold on a Life Technologies Veriti thermal cycler. All assays were validated by temperature gradient to ensure optimal separation of reference and variant signals. Data was analyzed using QuantaSoft v1.4 (Bio-Rad Laboratories). Positive control DNAs for each assay included NCI-

H441 (ATCC® HTB-174™) for *KRAS* c.35G>T;p.(Gly12Val) and synthetic construct gBlocks Gene Fragment (IDT, Coralville, Iowa, USA) for *KRAS* c.38G>T;p.(Gly13Val), *KRAS* c.436G>A;p.(Ala146Thr), *KRAS* c.183A>T;p.(Gln61His) and *HRAS* c.35G>A;p.(Gly12Asp). A positive control was not available for *KRAS* c.35G>A;p.(Gly12Asp). In addition, human genomic DNA (HuRef) plus one non-template control were genotyped with the study samples. Primers for ddPCR are shown in Table S4. We set a minimum of 0.5% fractional abundance to call a sample positive (similar to [6]).

DNA isolation and *KRAS* ddPCR from paraffin embedded and frozen samples in the Kuopio University Hospital replication cohort:

The replication cohort from Kuopio University Hospital (KUH) consisted of paraffin embedded BAVM samples (n=54), frozen BAVM samples (n=4), as well as paraffin embedded Circle of Willis samples (n=54) and cavernoma samples (n=8) that were used as controls. Thin (10-30 μm) sections were cut from paraffin embedded tissue samples using a microtome. The sections were deparaffinized with xylene for 3x15 min in 65^{o}C, rehydrated with a graded ethanol series and excessive ethanol removed by incubation at 40^{o}C. The tissue sections were then resuspended in 650 μL of DNA extraction buffer [5 mM EDTA, 250 mM NaCl, 1% SDS, 50 mM Tris, pH 7.6, and 0.2 mg/mL Proteinase K (Thermo Scientific, Waltham, MA)] and homogenized using Precellys Homogenizer (Bertin Instruments, Montigny-le-Bretonneux, France) (5500 rpm 2x30 sec) and soft tissue homogenizing CK14 tubes containing 1.4 mm ceramic (zirconium oxide) beads (Bertin Instruments). After incubation for 18 h at 50^{o}C under continuous agitation, the DNA was extracted with phenol:chloroform:isoamyl alcohol 25:24:1 (saturated with 10 mM Tris, pH 8.0; Amresco-inc, Solon, OH), followed by further purification with chloroform and then isopropanol precipitation. After two washes with 70% ethanol, the DNA was dissolved in nuclease-free H_2O and the DNA concentration measured using a NanoDrop spectrophotometer (NanoDrop products, Wilmington, DE). DNA isolation from KUH-derived frozen samples was performed similarly as described above for paraffin embedded samples, with the exception that no xylene or ethanol rehydration was needed and the samples were sectioned using a cryotome.

ddPCR for *KRAS* c.35G>A;p.(Gly12Asp) and c.35G>T;p.(Gly12Val) variants was performed from the DNA extracted from KUH-derived paraffin embedded and frozen samples as described previously for the original discovery cohort, with DNA concentrations of 50 or 250 ng of genomic DNA isolated from frozen samples or 250, 500, or 1000 ng of genomic DNA when

using DNA isolated from paraffin embedded samples. All the ddPCRs for c.35G>A;p.(Gly12Asp) and c.35G>T;p.(Gly12Val) were replicated at least two times, with the whole protocol repeated starting from the isolation of the genomic DNA. For most of the samples the c.35G>A;p.(Gly12Asp) ddPCRs were performed at least three times (Table S7). The ddPCR results of samples that did not have ≥ 500 droplets for *KRAS* wild-type in at least two replicates were considered unreliable and were excluded from further analysis (21/54 AVM samples). For larger AVM samples divided in several blocks, the DNA isolation and ddPCR was performed separately for each of the tissue blocks.

Since formalin-fixation can introduce false positives in *KRAS* c.35G>A;p.(Gly12Asp) ddPCR (as discovered also in our control samples from normal Circle of Willis and cavernomas), the c.35G>A;p.(Gly12Asp) ddPCR of all those samples that showed fractional abundance for c.35G>A;p.(Gly12Asp) above background level, were repeated using DNA that underwent uracil DNA glycosylase pretreatment, as described previously [7,8]. In brief, genomic DNA was incubated for 3 h at 37^{o}C with 2.5 μL (12.5 U) of uracil DNA glycosylase (New England BioLabs, Ipswich, MA) and 1 μL of 10x Reaction Buffer in a final volume of 10 μL. This pretreatment significantly reduced the background level (Table S7, Figure S3).

Cell culture of AVM and normal brain vascular endothelial cells:
Briefly, tissue was washed with PBS, sectioned into ~3 mm^2 fragments, and incubated with 0.1% collagenase (Sigma) at 37°C, for 20 min. Pre-digested tissue was triturated with a 2 mL pipette and filtered through a 100 μm cell strainer (BD Biosciences). The cell suspension was centrifuged at 2000 RPM for 5 min, and cells were washed and resuspended in EBM-2 media (Lonza), supplemented with EGM-2 MV SingleQuots (5% FBS, hydrocortisone, hFGF, VEGF, IGF-1, ascorbic acid, hEGF, GA-1000; Lonza).

ECs were isolated using anti-CD31 Dynabeads® (Life Technologies) according to the manufacturer's recommendations. CD31-positive and CD31-negative cell fractions were cultured in endothelial (EGM-2, Lonza) and smooth muscle (SmGM-2, Lonza) media, respectively, and used for further analyses. For immunocytochemistry, cells were fixed using 4% paraformaldehyde, permeabilized using 0.5% TX-100, and blocked using 5% normal goat serum (NGS). The rabbit polyclonal CD31 antibody (dilution, 1:20, cat. No. ab28364; Abcam, Cambridge, MA, USA) and the mouse monoclonal alpha SMA antibody (dilution, 1:400, cat. No. ab7817; Abcam) were added to the cells for 1.5 h at room temperature. Cells were washed 3

times, followed by 1 h incubation using goat anti-rabbit IgG, Alexa Fluor® 568 secondary antibody (dilution 1:500; cat. No. A11011; Thermofisher) or goat anti-mouse IgG, AlexaFluor® 488 (dilution 1:400; cat. No. A11029; Thermofisher) at room temperature. After further washing, coverslips were mounted in mounting media containing DAPI. Images were taken on a Zeiss AxioImager.M2 microscope, using a Hamamatsu digital camera.

Cell culture and treatment of human umbilical vein endothelial cells (HUVECs):
Primary endothelial cells were purchased from ScienCell and cultured according to manufacturer's instructions. Inhibitors of MEK (U0126, 20 μM, InvivoGen) or PI3K (LY294002, 10 μM, Cell Signaling) were added upon serum-starvation [0.1% FBS in basal media (ScienCell) with no additional growth factors] for 6 h. All drugs were dissolved in DMSO, and comparison was made to vehicle-treated (i.e. DMSO, 0.1%) controls. For experiments assessing the ability of MEK inhibition to rescue the adherens junction phenotype, confluent cells were treated with 20 μM U0126 for 18 h (in serum-starvation media).

Cell culture of telomerize-immortalized human aortic endothelial cells (TeloHAEC):
Cells were purchased from ATCC and grown in complete endothelial cell medium (Promocell).

Plasmids:
The following plasmids from Daniel Haber's lab were purchased from Addgene: #35634, pLenti-PGK-KRAS4A(G12V) and #35633, pLenti-PGK-KRAS4B(G12V). The open reading frames were amplified using primers that included an added BamHI site and a Kozak sequence on the 5' end and a XhoI site on the 3' end. PCR amplicons were then subcloned into $pCS2^{+}$ using the BamHI/XhoI sites. The LifeAct-GFP construct was from Ibidi. To assess electroporation efficiency (typically ~70%), pmaxGFP (Lonza) was co-electroporated in some experiments.

Electroporation:
~0.5 x 10^6 HUVECs were electroporated with 2.5 μg of pCS2, pCS2-$KRAS4A^{G12V}$ or pCS2-$KRAS4B^{G12V}$ constructs, together with 0.2 μg of pmaxGFP or 0.5 μg LifeAct-GFP using the P5 Primary Cell Kit (Lonza) and a 4D-nucleofector (Lonza). Cells were plated on one well of a 6-well dish or two wells of a 12-well dish, which were pre-coated with attachment factor (Thermo Scientific). Media was changed after 1 h.

Transfection of TeloHAEC:

Cells were transfected in OptiMEM medium at 60% confluency in 6-well plates using 2.5 μg of pCS2 or pCS2-KRAS4A^{G12V}, together with 0.2 μg of LifeAct-GFP and 10 μL of Lipofectamine 2000 (Invitrogen), according to the manufacturers' recommendations. After 4 h, transfection complexes were removed and replaced with complete medium (without antibiotics). After 24 h, cells were plated in 2-well LabTek coverglass plates (ThermoFisher, 155380) coated with attachment factor and incubated for 24 h prior to live imaging. 3 h prior to live imaging, cells were serum-starved in 0.1% FBS-containing medium without growth factors. Images were acquired on a Yokogawa Spinning Disk Confocal with a UPlanSApo 20x/0.75 NA objective. Cells were imaged every 3 minutes (10 μm stacks) for 3 hours.

Gene expression and cell biology experiments:

For gene expression studies, electroporated HUVECs were serum-starved the following day for 6 h, followed by RNA and protein isolation. In some experiments, small molecule inhibitors of signaling pathways were added. For cell biology experiments, cells were plated onto Permanox chamber slides the day after electroporation. Cells were serum-starved overnight prior to imaging. To assess cell migration, HUVEC were plated in 2-well culture inserts (Ibidi, Catalog #80209) on attachment factor-coated cover glass slides in complete media. Inserts were removed after 18 h and serum-starvation medium was added during 'scratch' repair. Cells were either fixed for static confocal imaging or were imaged using time-lapse confocal microscopy. To calculate cell migration rate, individual cells were tracked from time-lapse videos (5 h duration, 12 images/hour) taken during migration into the cell-free area of a 'scratch' assay. The distance between the starting and ending position of the cell was determined using the Manual Cell Tracking feature of Volocity software, and migration rate was determined by dividing this distance by the duration of migration. To assess cell proliferation, cells were serum-starved for 6 h, followed by addition of 10 μM BrdU (Sigma, Catalog #B5002) for 1 h at 37^{o}C. Cells were washed with PBS, fixed in 4% paraformaldehyde and permeabilized with 0.5% Triton X-100 in 10% DMSO, and quenched with 3% H_2O_2. Cells were then treated with DNase I (1:50 dilution, 4u/μL final concentration, 100 μL total volume, Invitrogen) at 37^{o}C for 1.5 h. Anti-BrdU-biotin (1:50 in blocking buffer, Biolegend, Catalog # 339810) was added overnight at 4^{o}C, followed by streptavidin-HRP (1:200 in blocking buffer, Perkin Elmer, Catalog #NEL750001EA) at room

temperature for 30 min. Tyramide-FITC (1:50, Perkin Elmer, Catalog #SAT701001EA) was added for 7 min at room temperature. After washing, slides were mounted in Vectashield containing DAPI (Vectorlabs, Catalog #H-100). The number of BrdU-positive nuclei was quantified using ImageJ in multiple random fields (40x objective, NA 0.8) and expressed as a percentage of total cell number. To assess cell survival, cells were cultured in complete or serum-stave medium for 24 h, followed by fixation in 4% paraformaldehyde and permeabilization in 0.5% Triton X-100 in 10% DMSO. TUNEL staining was performed using the In Situ Cell Death Detection kit (Roche, Catalog #11684795910), according to the manufacturer's recommendations. Slides were mounted in Vectashield containing DAPI, and the percentage of TUNEL-positive cells was determined as above.

Confocal microscopy:
Static imaging was performed using an Olympus FV1000 Confocal microscope using UplanSApo 20X/0.75NA, LumPlanFI40X/0.8NA, or Oil PlanApo 60X/1.42NA objectives. Time-lapse microscopy was performed using the WaveFX Yokogawa Spinning Disk Confocal with integrated environmental chamber, using UPlanSApo 20X/0.75NA or UPlanFL 10X/0.3NA objectives at a rate of 12 or 15 images per hour.

RNA isolation, and qRT-PCR:
RNA was isolated using Trizol.
Quantitative reverse-transcription PCR (qRT-PCR) - Following DNase I treatment (Invitrogen), reverse transcription was performed on 1 μg of RNA using the High Capacity cDNA Synthesis Kit (Thermo Scientific). qRT-PCR was performed using a Roche Lightcycler 480® with LC 480 SYBR Green I Master Mix (Roche). Data were normalized to Tata Box Binding Protein (TBP) using the Δ - Δ Ct method. Primer sequences are listed in Table S10.

Immunofluorescence:
HUVEC were grown on attachment factor-coated Permanox or glass chamber slides (Nunc-LabTek). Cells were fixed with 4% paraformaldehyde followed by permeabilization with 0.25% Triton X-100. Staining with anti-pERK (rabbit polyclonal, Cell Signaling, #9101, 1:500) or anti-VE-Cadherin (R&D Systems, #MAB9381) was performed overnight at 4°C, followed by secondary antibody addition (anti-rabbit-AlexaFluor647, Thermo Scientific, #A21235). Slides

were mounted using Vectashield mounting medium with DAPI (Vector Labs, #H-1200) and imaged using an Olympus FV1000 Confocal microscope.

SDS-PAGE and Immunoblotting:
Protein lysates from cultured cells were homogenized in lysis buffer (250 mM NaCl, 20 mM HEPES, 30 mM $MgCl_2$, 0.5 mM EDTA, 0.1 mM EGTA, 20% glycerol, 1% NP-40) supplemented with 0.25 mM DTT, 0.1 mg/mL AEBSF, phosphatase- and protease-inhibitor cocktails, and centrifuged at 14,000 xg, for 10 min at 4°C. Protein concentration was determined using the BioRad protein assay. 40 μg of protein was separated by SDS-PAGE, followed by transfer to PVDF membrane. The following antibodies were used: rabbit anti-AKT (Cell Signaling, Cat. #9272), rabbit anti-phospho-AKT(S473) (SAB, Cat. #11054), rabbit anti-ERK1/2 (Cell Signaling, Cat. #9102), rabbit anti-phospho-ERK(T202/T204) (Cell Signaling, Cat. #9101), rabbit anti-p38 (Cell Signaling, Cat. #9212), rabbit anti-phospho-p38(T180/T182) (Cell Signaling, Cat. #9211), rabbit anti-B-actin (Cell Signaling, Cat. #5125).

Immunohistochemistry:

4 μm FFPE sections of 25 BAVMs included in this study (with and without *KRAS* mutations detected by ddPCR) were stained with phospho-ERK. Paraffin-embedded sections were dewaxed in 5 changes of xylene and rehydrated to water through graded alcohol washes. Heat induced epitope retrieval in 10 mM citrate buffer (pH 6.0) was used and endogenous peroxidase blocked with 3% hydrogen peroxide. The antibody to phosho-ERK (Cell Signaling; Cat. #9101) was used at a dilution of 1:800 overnight. The detection system used was species-specific ImmPRESS polymer system Anti-Rabbit IgG Cat# MP-7401 (Vector Labs). After following kit instructions, color development was performed with freshly prepared DAB (DAKO Cat# K3468). Finally, sections were counterstained lightly with Mayer's Hematoxylin, dehydrated in alcohols, cleared in xylene and mounted with Permount mounting medium (Fisher, cat# SP15-500).

RNA sequencing:
RNA sequencing was done at the Princess Margaret Genomics Center, Toronto, Canada. Total RNA was extracted from HUVEC electroporated with pCS2, pCS2-KRAS4A^{G12V} and pCS2-KRAS4B^{G12}. 200 ng of RNA was used to synthesize cDNA. RNA samples were quantified by Qubit (Life Technologies) and by Bioanalyzer (Agilent). All samples had RIN above 8. Libraries

were prepared using TruSeq Stranded Total RNA kit (Illumina). 200 ng from RNA samples were ribosomal RNA depleted using Ribo-zero Gold rRNA beads, and following purification the RNA was fragmented. The cleaved RNA fragments were copied into first strand cDNA using reverse transcriptase and random primers. This was followed by second strand cDNA synthesis using RNase H and DNA Polymerase I. A single "A" base was added and adapter ligated followed by purification and enrichment with PCR to create cDNA libraries. Final cDNA libraries were size validated by Bioanalyzer and concentration was validated by qPCR. All uniquely bar-coded cDNA libraries were normalized to 10 nM and pooled together. 10 pM of pooled libraries were loaded onto an Illumina cBot for cluster generation. The clustered flow cell was then sequenced (paired-end, 100 cycles V3) using an Illumina HighSeq 2000 to achieve a minimum of ~35 million reads per sample. Overall read quality was checked using FASTQC v.0.11.2 and for RNA QC the tool RNA-SeQC (v1.1.7) was used. Raw sequence data, in the form of FASTQ files, was aligned to the human genome (hg19, iGenome GTF definition file) using the BOWTIE/TOPHAT pipeline (BOWTIE v2.2.6, TOPHAT 2.1.0). Accessory programs for the alignment stage include SAMTOOLS (v1.2) and Flexbar (2.5.0). Transcript assembly, abundance estimation, and tests for differential regulation were done using CUFFLINKS (v2.2.1)

GSEA analysis

Gene Set Enrichment analysis was performed using the GSEA software [9] (corrected p-value was obtained after 10000 permutations of the gene sets). Comparison was made between RNA-sequencing data from HUVEC over-expressing KRAS4A^{G12V} or KRAS4B^{G12V} and data from HUVEC stimulated with VEGF for 1 h (GEO dataset: GSE41166) [10].

References

1. Li H, Durbin R. Fast and accurate long-read alignment with Burrows-Wheeler transform. Bioinformatics 2010;26:589-95.

2. McKenna A, Hanna M, Banks E, et al. The Genome Analysis Toolkit: a MapReduce framework for analyzing next-generation DNA sequencing data. Genome Res 2010;20:1297-303.

3. Cibulskis K, Lawrence MS, Carter SL, et al. Sensitive detection of somatic point mutations in impure and heterogeneous cancer samples. Nat Biotechnol 2013;31:213-9.

4. Adzhubei I, Jordan DM, Sunyaev SR. Predicting functional effect of human missense mutations using PolyPhen-2. Curr Protoc Hum Genet 2013;Chapter 7:Unit7 20.

5. Limaye N, Kangas J, Mendola A, et al. Somatic Activating PIK3CA Mutations Cause Venous Malformation. Am J Hum Genet 2015;97:914-21.

6. Luks VL, Kamitaki N, Vivero MP, et al. Lymphatic and other vascular malformative/overgrowth disorders are caused by somatic mutations in PIK3CA. J Pediatr 2015;166:1048-54 e1-5.

7. Do H, Dobrovic A. Dramatic reduction of sequence artefacts from DNA isolated from formalin-fixed cancer biopsies by treatment with uracil- DNA glycosylase. Oncotarget 2012;3:546-58.

8. Serizawa M, Yokota T, Hosokawa A, et al. The efficacy of uracil DNA glycosylase pretreatment in amplicon-based massively parallel sequencing with DNA extracted from archived formalin-fixed paraffin-embedded esophageal cancer tissues. Cancer Genet 2015;208:415-27.

9. Subramanian A, Tamayo P, Mootha VK, et al. Gene set enrichment analysis: a knowledge-based approach for interpreting genome-wide expression profiles. Proc Natl Acad Sci U S A 2005;102:15545-50.

10. Zhang B, Day DS, Ho JW, et al. A dynamic H3K27ac signature identifies VEGFA-stimulated endothelial enhancers and requires EP300 activity. Genome Res 2013;23:917-27.

Supplemental Tables

Table S1: Excel spreadsheet showing MuTec2 results for the 6 coding missense variants including 4 variants causing a *KRAS* c.35G>A;p.(Gly12Asp) mutation in 4 patients [Included as a separate Excel file]

Table S2: Summary of *KRAS* variants found with exome sequencing of the Toronto cohort using two algorithms, MuTecT2 and Variant Checker

* variants reported by MuTect2 with a "Rejected" flag if their VAFs were below 3%. Nidus: samples taken from the BAVM nidus. DV: sample taken from the draining vein. ()= number of reads

Patient	Tissue	CONTROL	MUTECT2_DR100	Variant Checker_KRAS
1	Nidus	yes	KRAS_c.35G>A;p.(Gly12Asp)_2.4%_(7)	KRAS_c.35G>A;p.(Gly12Asp)_2%_(6/0)
1	DV	yes	KRAS_c.35G>A;p.(Gly12Asp)_1%_(4)	KRAS_c.35G>A;p.(Gly12Asp)_1.3%_(3/3)
2	Nidus	yes	KRAS_c.35G>T;p.(Gly12Val)_3%_(9)	KRAS_c.35G>T;p.(Gly12Val)_3.4%_(7/2)
3	Nidus	yes		KRAS_c.35G>A;p.(Gly12Asp)_0.9%_(1/2)
4	Nidus	yes	KRAS_c.35G>A;p.(Gly12Asp)_4%_(13)	KRAS_c.35G>A;p.(Gly12Asp)_4.2%_(9/4)
5	Nidus	no	KRAS_c.35G>T;p.(Gly12Val)_3.2%_(8)	KRAS_c.35G>T;p.(Gly12Val)_3.2%_(8/1)
6	Nidus	yes	KRAS_c.35G>A;p.(Gly12Asp)_1.7%_(5)*	KRAS_c.35G>A;p.(Gly12Asp)_1.5%_(4/1)
7	Nidus	yes	KRAS_c.35G>T;p.(Gly12Val)_2%_(4)*	KRAS_c.35G>T;p.(Gly12Val)_1.8%_(3/1)
8	Nidus	yes		
9	Nidus	no		KRAS_c.38G>T;p.(Gly13Val)_0.9%_(1/1)
9	Nidus	no		KRAS_c.35G>T;p.(Gly12Val)_1.3%_(1/2)
10	Nidus	yes	KRAS_c.35G>A;p.(Gly12Asp)_3.3%_(13)	KRAS_c.35G>A;p.(Gly12Asp)_3.1%_(7/6)
11	Nidus	yes		
12	Nidus	no		
13	Nidus	no		
14	Nidus	yes		KRAS_c.35G>A;p.(Gly12Asp)_1.4%_(3/1)
15	Nidus	no		KRAS_c.35G>A;p.(Gly12Asp)_0.9%_(1/2)
16	Nidus	yes		
17	Nidus	yes		
18	Nidus	no		KRAS_c.35G>A;p.(Gly12Asp)_1.3%_(2/1)
19	Nidus	yes		
20	Nidus	no		KRAS_ c.183A>T;p.(Gln61His)_4.1%_(1/1)
21	Nidus	yes		
22	Nidus	yes		
23	Nidus	yes		
24	Nidus	no		KRAS_p.Gly13Cys_0.6%_(1/1)
25	Nidus	yes		
26	Nidus	no		

Table S3: Summary of somatic variants of *KRAS* in brain arteriovenous malformation tissue samples from Toronto and Kuopio.

FFPE: formalin fixed paraffin embedded, NV: normal vessels (NV1, NV2, NV3 were used for cell cultures shown in Figure 3A and S4. For NV1 and NV2, no whole tissue was available for analysis). AVF: arteriovenous fistula, CCM: cerebral cavernous malformation

Toronto Cohort (fresh frozen samples)						**Finnish Cohort (FFPE)**			
Patient	**Sample**	**Whole Exome Sequencing**		**droplet digital PCR**		**Patient**	**Blocs**	**droplet digital PCR**	
		allelic frequency (%)	***KRAS* variant**	**fractional abundance (%)**	***KRAS* variant**		+/total	**fractional abundance (%)**	***KRAS* variant**
1	**nidus**	2	c.35G>A; p.(Gly12Asp)	2.88	c.35G>A; p.(Gly12Asp)	**1**	0/1	-	-
1	**Vein**	1.3	c.35G>A; p.(Gly12Asp)	1.67	c.35G>A; p.(Gly12Asp)	**2**	0/1	-	-
1	**blood**	-	-	-	-	**3**	0/2	-	-
2	**nidus**	3.4	c.35G>T; p.(Gly12Val)	3.17	c.35G>T; p.(Gly12Val)	**4**	1/1	1.4	c.35G>A; p.(Gly12Asp)
2	**blood**	-	-	-	-	**5**	1/1	3.6	c.35G>A; p.(Gly12Asp)
3	**nidus**	0.9	c.35G>T; p.(Gly12Val)	1.43	c.35G>A; p.(Gly12Asp)	**6**	0/6	-	-
3	**blood**	-	-	-	-	**7**	0/4	-	-
4	**nidus**	4.2	c.35G>A; p.(Gly12Asp)	4.37	c.35G>A; p.(Gly12Asp)	**8**	0/3	-	-
4	**blood**	-	-	-	-	**9**	2/2	2.15	c.35G>A; p.(Gly12Asp)
5	**nidus**	3.2	c.35G>T; p.(Gly12Val)	3	c.35G>T; p.(Gly12Val)	**10**	1/1	3.19	c.35G>A; p.(Gly12Asp)
6	**nidus**	1.5	c.35G>A; p.(Gly12Asp)	2.98	c.35G>A; p.(Gly12Asp)	**11**	1/1	1.35	c.35G>T; p.(Gly12Val)
6	**blood**	-	-	-	-	**12**	0/5	-	-
7	**nidus**	1.8	c.35G>T; p.(Gly12Val)	2.46	c.35G>T; p.(Gly12Val)	**13**	1/1	3.45	c.35G>A; p.(Gly12Asp)
7	**blood**	-	-	-	-	**14**	1/2	1.28	c.35G>T; p.(Gly12Val)
8	**nidus**	-	-	2.41	c.183A>T; p.(Gln61His)	**15**	0/1	-	-
8	**blood**	-	-	-	-	**16**	1/2	0.7	c.35G>T; p.(Gly12Val)
9	**nidus**	1.3	c.35G>T; p.(Gly12Val)	1.56	c.35G>T; p.(Gly12Val)	**17**	1/1	1.05	c.35G>A; p.(Gly12Asp)
9	**blood**	-	-	-	-	**18**	1/1	1.31	c.35G>A; p.(Gly12Asp)
10	**nidus**	3.1	c.35G>A; p.(Gly12Asp)	2.4	c.35G>A; p.(Gly12Asp)	**19**	0/1	-	-

11	**nidus**	-	-	0.5	c.35G>T; p.(Gly12Val)	**20**	1/1	1.80	c.35G>T; p.(Gly12Val)
11	**blood**	-	-	-	-	**21**	2/2	2.08	c.35G>A; p.(Gly12Asp)
12	**nidus**	-	-	1.44	c.35G>T; p.(Gly12Val)	**22**	2/4	1.68	c.35G>A; p.(Gly12Asp)
13	**nidus**	-	-	1.16	c.35G>T; p.(Gly12Val)	**23**	0/1	-	-
14	**nidus**	1.4	c.35G>A; p.(Gly12Asp)	0.62	c.35G>A; p.(Gly12Asp)	**24**	0/1	-	-
14	**blood**	-	-	-	-	**25**	0/1	-	-
15	**nidus**	0.9	c.35G>A; p.(Gly12Asp)	1.66	c.35G>A; p.(Gly12Asp)	**26**	0/3	-	-
16	**nidus**	-	-	0.64	c.35G>A; p.(Gly12Asp)	**27**	1/1	3.00	c.35G>A; p.(Gly12Asp)
17	**nidus**	-	-	2.19	c.35G>A; p.(Gly12Asp)	**28**	0/1	-	-
17	**blood**	-	-	-	-	**29**	1/1	1.24	c.35G>A; p.(Gly12Asp)
18	**nidus**	1.3	c.35G>A; p.(Gly12Asp)	0.76	c.35G>A; p.(Gly12Asp)	**30**	0/1	-	-
18	**blood**	-	-	-	-	**31**	0/3	-	-
19	**nidus**	-	-	-	-	**32**	1/1	2.20	c.35G>A; p.(Gly12Asp)
19	**blood**	-	-	-	-	**33**	0/1	-	-
20	**nidus**	n/a	n/a	-	-			**Finnish Cohort**	**(Fresh Frozen)**
21	**nidus**	-	-	-	-	Patient	Blocs	FA	*KRAS* variant
22	**nidus**	-	-	-	-	2	0/1	-	-
22	**blood**	-	-	-	-	3	0/1	-	-
23	**nidus**	-	-	-	-	10	1/1	0.87	c.35G>A; p.G12D
23	**blood**	-	-	-	-				
24	**nidus**	-	-	-	-				
24	**blood**	-	-	-	-				
25	**nidus**	-	-	-	-				
26	**nidus**	-	-	-	-				
26	**blood**	-	-	-	-				
27	**nidus**	-	-	-	-				
28	**nidus**	n/a	n/a	6.72	c.35G>A; p.(Gly12Asp)				
29	**nidus**	n/a	n/a	0.763	c.35G>A; p.(Gly12Asp)				
30	**nidus**	n/a	n/a	1.6	c.35G>T; p.(Gly12Val)				

31	**nidus**	n/a	n/a	0.753	c.35G>A; p.(Gly12Asp)				
32	**nidus**	n/a	n/a	n/a	n/a				
33	**nidus**	n/a	n/a	1.4	c.35G>A; p.(Gly12Asp)				
33	**blood**	n/a	n/a	-	-				
34	**nidus**	n/a	n/a	0.43	c.35G>A; p.(Gly12Asp)				
34	**blood**	n/a	n/a	-	-				
35	**nidus**	n/a	n/a	1.7	c.35G>T; p.(Gly12Val)				
35	**blood**	n/a	n/a	-	-				
36	**nidus**	n/a	n/a	1.09	c.35G>A; p.(Gly12Asp)				
36	**blood**	n/a	n/a	-	-				
37	**nidus**	n/a	n/a	1.34	c.35G>A; p.(Gly12Asp)				
38	**nidus**	n/a	n/a	-	-				
38	**blood**	n/a	n/a	n/a	n/a				
39	**nidus**	n/a	n/a	2.34	c.35G>A; p.(Gly12Asp)				
39	**vein**	n/a	n/a	0.283	c.35G>A; p.(Gly12Asp)				
39	**blood**	n/a	n/a	n/a	n/a				
Normal Vessels -Toronto Cohort (fresh frozen samples)						**Normal Vessels-Finnish Cohort (FFPE)**			
Patient	**Sample**	**Whole Exome Sequencing**		**droplet digital PCR**		**Patient**	**Blocs**	**droplet digital PCR**	
		allelic frequency (%)	***KRAS* variant**	**fractional abundance (%)**	***KRAS* variant**		+/total	**fractional abundance (%)**	***KRAS* variant**
1	NV1	n/a	n/a	n/a	n/a	**All patients (1 to 54)**		-	-
2	NV2	n/a	n/a	n/a	n/a				
3	NV3	n/a	n/a	-	-				
4	NV4	n/a	n/a	-	-				
Non-AVM Disease -Toronto Cohort (fresh frozen samples)						**Non-AVM Disease-Finnish Cohort (FFPE)**			
Patient	**Sample**	**Whole Exome**		**droplet digital PCR**		**Patient**	**Blocs**	**droplet digital PCR**	

		Sequencing							
		allelic frequency (%)	***KRAS* variant**	**fractional abundance (%)**	***KRAS* variant**		+/total	**fractional abundance (%)**	***KRAS* variant**
1	**AVF**	n/a	n/a	-	-	**1 (AVF)**	0/1	-	-
2	**CCM**	n/a	n/a	-	-	**2 (AVF)**	0/3	-	-
3	**CCM**	n/a	n/a	-	-	**3 (CCM)**	0/1	-	-
						4 (CCM)	0/1	-	-
						5 (CCM)	0/1	-	-
						6 (CCM)	0/1	-	-
						7 (CCM)	0/1	-	-
						9 (CCM)	0/4	-	-
						10 (CCM)	0/3	-	-
						11 (CCM)	0/1	-	-
						12 (CCM)	0/1	-	-
						13 (CCM)	0/2	-	-
						15 (CCM)	0/1	-	-
						16 (CCM)	0/1	-	-
						18 (CCM)	0/1	-	-
						19 (CCM)	0/1	-	-
						20 (CCM)	0/4	-	-

Table S4: Primers used for ddPCR analyses

KRAS c.35G>A;p.(Gly12Asp)	
Forward Primer	AGGCCTGCTGAAAATGACTGAATAT
Reverse Primer	GCTGTATCGTCAAGGCACTCTT
Reporter 1 (VIC) sequence	TTGGAGCTG**G**TGGCGTA
Reporter 2 (FAM) sequence	TTGGAGCTG**A**TGGCGTA
KRAS c.35G>T;p.(Gly12Val)	
Forward Primer	AGGCCTGCTGAAAATGACTGAATAT
Reverse Primer	GCTGTATCGTCAAGGCACTCTT
reporter 1 (VIC) sequence	TTGGAGCTG**G**TGGCGTA
reporter 2 (FAM) sequence	TTGGAGCTG**T**TGGCGTA
KRAS c.38G>T;p.(Gly13Val)	
Forward Primer	AGCTGTATCGTCAAGGCACTCTT
Reverse Primer	GGCCTGCTGAAAATGACTGAA
Reporter 1 (VIC) sequence	CCTACG**C**CACCAGCT
Reporter 2 (FAM) sequence	CTACG**A**CACCAGCT
HRAS c.35G>A;p.(Gly12Asp)	
Forward Primer	CACAAAATGGTTCTGGATCAGC
Reverse Primer	CGATGACGGAATATAAGCTGGTG
Reporter 1 (VIC) sequence	TTGCCCACACCG**C**CG
Reporter 2 (FAM) sequence	CTTGCCCACACCG**T**CG

KRAS c.183A>T;p.(Gln61His) and *KRAS* c.436G>A;p.(Ala146Thr) validated TaqMan® SNP Genotyping Assays for digital PCR were obtained from Life Technologies (Part 4332077, Assay IDs: AHFA90M and AHWSLAG, respectively).

Table S5: Excel spreadsheet showing the number of positive events and the number of wild-type and total events for every Toronto BAVM sample tested by *KRAS* c.35G>T;p.(Gly12Val)- or c.35G>A;p.(Gly12Asp)-specific ddPCR [Included as a separate Excel file]

Table S6: Summary of clinical data and *KRAS* status of Fresh Frozen Toronto patients
Summary of the clinical presentation and *KRAS* c.35G>A;p.(Gly12Asp), c.35G>T;p.(Gly12Val) and *KRAS* c.183A>T;p.(Gln61His) status of Toronto patients and their BAVM samples.

PATIENT	age	Gender	KRAS mutation	Rupture	Location	size 1 (0-3cm), 2(3-6cm), 3 (>6cm)	venous drainage	Prior Radiation
1	26	M	G12D	yes	cingulate	2	deep	no
2	23	M	G12D	yes	temporal	1	deep	yes
3	21	M	G12V	yes	cerebellar	1	both	yes
4	18	F	G12D	no	parieto-occipital	1	superficial	no
5	42	F	G12V	no	frontal	2	superficial	no
6	18	M	G12D	no	frontal	1	superficial	no
7	53	F	G12V	no	temporal	2	superficial	no
8	39	F	Q61H	no	occipital	2	both	no
9	26	M	G12V	yes	parietal	1	superficial	no
10	26	M	G12D	no	frontal	2	deep	no
11	42	F	G12V	yes	occipital	1	superficial	no
12	66	M	G12V	yes	temporal	1	superficial	no
13	59	F	G12V	no	temporal	2	superficial	no
14	17	F	G12D	no	temporal	1	deep	no
15	29	M	G12D	yes	frontal	1	superficial	no
16	59	M	G12D	yes	frontal	1	superficial	no
17	34	F	G12D	no	frontal	1	superficial	no
18	19	F	G12D	yes	cerebellar	2	superficial	no
19	26	M	neg	yes	occipital	1	deep	no
20	52	F	neg	yes	parietal	3.0	both	no
21	29	M	neg	yes	temporal	1	superficial	no
22	32	F	neg	no	frontal	1	both	no
23	27	F	neg	no	frontal	2	superficial	no
24	59	F	neg	yes	parietal	1	superficial	yes
25	56	M	neg	no	temporal	1	superficial	no
25	25	M	neg	yes	temporal	1	superficial	yes
26	48	F	neg	no	parietal	2	superficial	no
28	32	F	G12D	no	insular	1	superficial	no
29	25	F	G12D	no	frontal	2	both	no
30	75	M	G12V	yes	cerebellar	2	both	yes
31	40	M	G12D	no	parieto-occipital	1	deep	no
32	46	M		yes	frontal	1	superficial	no
33	48	F	G12D	yes	frontal	1	both	no
34	27	M	G12D	yes	frontal	1.0	superficial	no
35	25	F	G12V	no	occipital	1.0	superficial	yes
36	46	M	G12D	yes	parieto-occipital	1.0	superficial	no
37	58	F	G12D	no	occipital	2.0	superficial	no
38	53	F	neg	yes	frontal	2	both	no
39	58	M	G12D	yes	parietal	2.0	superficial	no

Table S7: Excel spreadsheet showing the number of positive events and the number of wild-type events for every Kuopio sample tested by ddPCR, including UDC treatment of FFPE BAVM and control vascular samples [Included as a separate Excel file]
The amount of genomic DNA in the ddPCR reactions was 500 ng unless otherwise indicated in *italic*, in which case 250 ng was used.

Table S8: Summary of clinical data and ddPCR results of Finnish FFPE BAVM samples
Summary of the clinical presentation and *KRAS* c.35G>A;p.(Gly12Asp) and c.35G>T;p.(Gly12Val) ddPCR results for the KUH replication cohort. * Fractional abundance is presented as mean and range (min-max) of all those PCRs performed on the sample that gave a WT replication of >500 copies

Patient	Age	Sex	Rupture	Epilepsy at presentation	Location	Size 1=<3cm, 2=3-6cm, 3>6cm	Venous drainage	Prior radiation	KRAS variant	Fractional abundance G12D	G12D ddPCRs	Fractional abundance G12V	G12V ddPCRs	Mutation + /all blocks
1	42	F	yes	no	Occipito-parietal	1	superficial	no	neg	0.20 (0.04-0.32)	4	0.00 (0.00-0.00)	2	0/1
2	60	M	yes	no	Temporal	1	superficial	no	neg	0.12 (0.09-0.14)	3	0.04 (0.02-0.06)	2	0/1
3	39	F	no	no	Occipital	1	superficial	no	neg	0.27 (0.12-0.50)	3	0.04 (0.00-0.11)	2	0/2
4	32	M	yes	no	Occipital	1	superficial	no	**G12D**	**1.40 (1.20-1.60)**	3	0.04 (0.00-0.07)	2	**1/1**
5	31	F	yes	no	Frontal	1	superficial	no	**G12D**	**3.60 (3.40-3.70)**	3	0.07 (0.00-0.13)	2	**1/1**
6	41	F	no	no	Occipital	2	superficial	yes	neg	0.24 (0.00-0.80)	2-4	0.02 (0.00-0.15)	2	0/6
7	57	M	no	no	Occipital	1	deep	no	neg	0.26 (0.00-0.60)	3-6	0.00 (0.00-0.00)	2	0/4
8	13	F	yes	yes	Frontal	2	superficial	no	neg	0.06 (0.00-0.11)	4	0.00 (0.00-0.00)	2	0/3
9	40	F	yes	no	Frontal	1	deep	no	**G12D**	**2.15 (1.73-2.70)**	4	0.00 (0.00-0.00)	2	**2/2**
10	62	M	yes	yes	Fronto-parietal	1	superficial	no	**G12D**	**3.19 (2.70-3.50)**	4	0.00 (0.00-0.01)	2	**1/1**
11	52	M	yes	no	Parietal	3	superficial	no	**G12V**	0.25 (0.19-0.30)	2	**1.35 (0.94-1.90)**	3	**1/1**
12	21	F	yes	no	Frontal	1	superficial	no	neg	0.12 (0.00-0.20)	3-4	0.00 (0.00-0.00)	2	0/5
13	42	M	yes	no	Occipital	1	superficial	no	**G12D**	**3.45 (1.90-4.42)**	3	0.00 (0.00-0.00)	2	**1/1**
14	48	M	yes	yes	Parietal	1	superficial	no	**G12V**	0.50 (0.31-0.87)	2	**1.28 (0.70-2.10)**	4	**1/2**
15	36	M	yes	no	Temporal	1	superficial	no	neg	0.17 (0.00-0.33)	2	0.00 (0.00-0.00)	2	0/1
16	45	M	yes	no	Fronto-temporo-parietal	1	superficial	no	**G12V**	0.32 (0.20-0.46)	2-3	**0.70 (0.41-1.00)**	4	**1/2**
17	38	F	yes	no	Occipital	1	superficial	no	**G12D**	**1.05 (0.86-1.40)**	3	0.02 (0.00-0.04)	2	**1/1**
18	38	M	yes	no	Parietal	1	not known	no	**G12D**	**1.31 (1.28-1.33)**	3	0.01 (0.00-0.02)	2	**1/1**
19	45	F	no	no	Parietal	1	not known	no	neg	0.31 (0.14-0.48)	2	0.12 (0.00-0.23)	3	0/1
20	36	F	yes	no	Sylvian fissure /temporal	1	deep & superficial	no	**G12V**	0.49 (0.19-0.69)	2	**1.80 (1.10-1.80)**	3	**1/1**
21	21	F	no	yes	Frontal	2	superficial	no	**G12D**	**2.08 (1.20-3.40)**	3	0.00 (0.00-0.00)	2	**2/2**
22	12	F	yes	no	Frontal	uncertain	deep & superficial	no	**G12D**	**1.68 (0.80-2.40)**	2-3	0.00 (0.00-0.00)	2	**2/4**
23	14	F	yes	no	Frontal	1	superficial	no	neg	0.37 (0.26-0.48)	2	0.05 (0.00-0.11)	2	0/1
24	29	F	no	yes	Temporobasal	3	deep & superficial	no	neg	0.23 (0.14-0.31)	2	0.02 (0.00-0.04)	2	0/1
25	60	M	no	yes	Frontal	1	superficial	no	neg	0.13 (0.00-0.20)	2	0.07 (0.00-0.29)	2-3	0/1
26	52	F	yes	no	Frontoparietal	3	superficial	yes	neg	0.39 (0.17-0.80)	2	0.00 (0.00-0.00)	2	0/3
27	4	F	yes	no	Parietal	1	superficial	no	**G12D**	**3.00 (2.90-3.10)**	3	0.00 (0.00-0.00)	2	**1/1**
28	64	F	yes	yes	Occipital	1	superficial	no	neg	0.31 (0.26-0.36)	2	0.01 (0.00-0.03)	2	0/1
29	33	F	no	no	Sylvian fissure	1	superficial	no	**G12D**	**1.24 (1.06-1.45)**	3	0.00 (0.00-0.00)	2	**1/1**
30	22	M	yes	no	Thalamic	2	deep	no	neg	0.43 (0.38-0.48)	2	0.03 (0.01-0.05)	2	0/1
31	50	M	yes	no	Sylvian fissure / parietal	2	superficial	no	neg	0.25 (0.07-0.60)	2-3	0.01 (0.00-0.08)	2	0/3
32	65	M	no	no	Sylvian fissure / frontal	1	superficial	no	**G12D**	**2.20 (1.90-2.70)**	3	0.04 (0.00-0.07)	2	**1/1**
33	25	M	yes	no	Frontal / basal ganglia	uncertain	deep	no	neg	0.29 (0.28-0.29)	2	0.00 (0.00-0.00)	2	0/1

Table S9: ddPCR results and fractional abundance of *KRAS* variants in MAC-sorted CD31$^+$ and CD31$^-$ fractions of primary vascular cell cultures of BAVMs and normal brain vessels.

Note that all material from AVM tissue from Patient #32 was used for MAC-sorting, so analysis of the AVM itself was not possible.

Sample	Fractional Abundance (%)	KRAS variant
AVM 1 tissue (Patient #29)	0.763	c.35G>A; p.(Gly12Asp)
AVM 2 tissue (Patient #30)	1.6	c.35G>T; p.(Gly12Val)
AVM 3 tissue (Patient #31)	0.753	c.35G>A; p.(Gly12Asp)
AVM 4 tissue (Patient #32)	n/a	n/a
AVM 5 tissue (Patient #38)	0.0	0.0
AVM 6 tissue (Patient #39)	Vein: 0.283 Nidus: 2.34	c.35G<T; p.(Gly12Asp)
AVM 1 CD31+ (Patient #29)	4.38	c.35G>A; p.(Gly12Asp)
AVM 2 CD31+ (Patient #30)	14.9	c.35G>T; p.(Gly12Val)
AVM 3 CD31+ (Patient #31)	2.13	c.35G>A; p.(Gly12Asp)
AVM 4 CD31+ (Patient #32	45.8	c.35G>A; p.(Gly12Asp)
AVM 5 CD31+ (Patient #38)	0.0	0.0
AVM 6 CD31+ (Patient #39)	Vein: 30.5 Nidus: 52.1	c.35G>A; p.(Gly12Asp)
AVM 1 CD31- (Patient #29)	0.0	0.0
AVM 2 CD31- (Patient #30)	0.0	0.0
AVM 3 CD31- (Patient #31)	0.0	0.0
AVM 4 CD31- (Patient #32)	0.0	0.0
AVM 5 CD31- (Patient #38)	0.0	0.0
AVM 6 CD31- (Patient #39)	0.0	0.0
NV 1 CD31+	0.0	0.0
NV 2 CD31+	0.0	0.0
NV 3 CD31+	0.0	0.0
NV 1 CD31-	0.0	0.0
NV 2 CD31-	0.0	0.0
NV 3 CD31-	0.0	0.0

KRAS variants c.35G>A;p.(Gly12Asp) or c.35G>T;p.(Gly12Val) are found in 5 of 6 endothelium enriched, CD31$^+$ cultures, but are absent in endothelium-depleted, CD31$^-$ BAVM fractions, or in either fractions of normal brain vessel cultures.

Table S10: Primers used for qRT-PCR analyses

Gene	Forward Primer	Reverse Primer
BHLHE40	CCT TGA AGC ATG TGA AAG CA	CAT GTC TGG AAA CCT GAG CA
DUSP1	CCA ACC ATT TTG AGG GTC AC	ACC CTT CCT CCA GCA TTC TT
DUSP5	ATG GAT CCC TGT GGA AGA CA	TCA CAG TGG ACC AGG ACC TT
DUSP6	CTG TCG ATG AAC GAT GCC TA	AGC AGC TGA CCC ATG AAG TT
EGR1	CAG CAC CTT CAA CCC TCA G	TAA CTG GTC TCC ACC AGC AC
HES1	CGG ACA TTC TGG AAA TGA CA	GTC ACC TCG TTC ATG CAC TC
IL1A	TGT GAC TGC CCA AGA TGA AG	CCG TGA GTT TCC CAG AAG AA
SIK1	CAG TAG GCA CCC GAG CAG	CGC TGA ACT CCG ACA TGA TA
SPRY4	TCC GTA CAG TCC AGG ACC TC	GGC TGG ACC ATG ACT GAG TT
TBP	CTC CAC GGA GGA GAG AAC C	AAG CAT CAT CTT CCC CCT TC
TRIB1	TCG GAG AGT TCT GGG ATT GT	CAC GAA GTG CAA TGG TCT TT

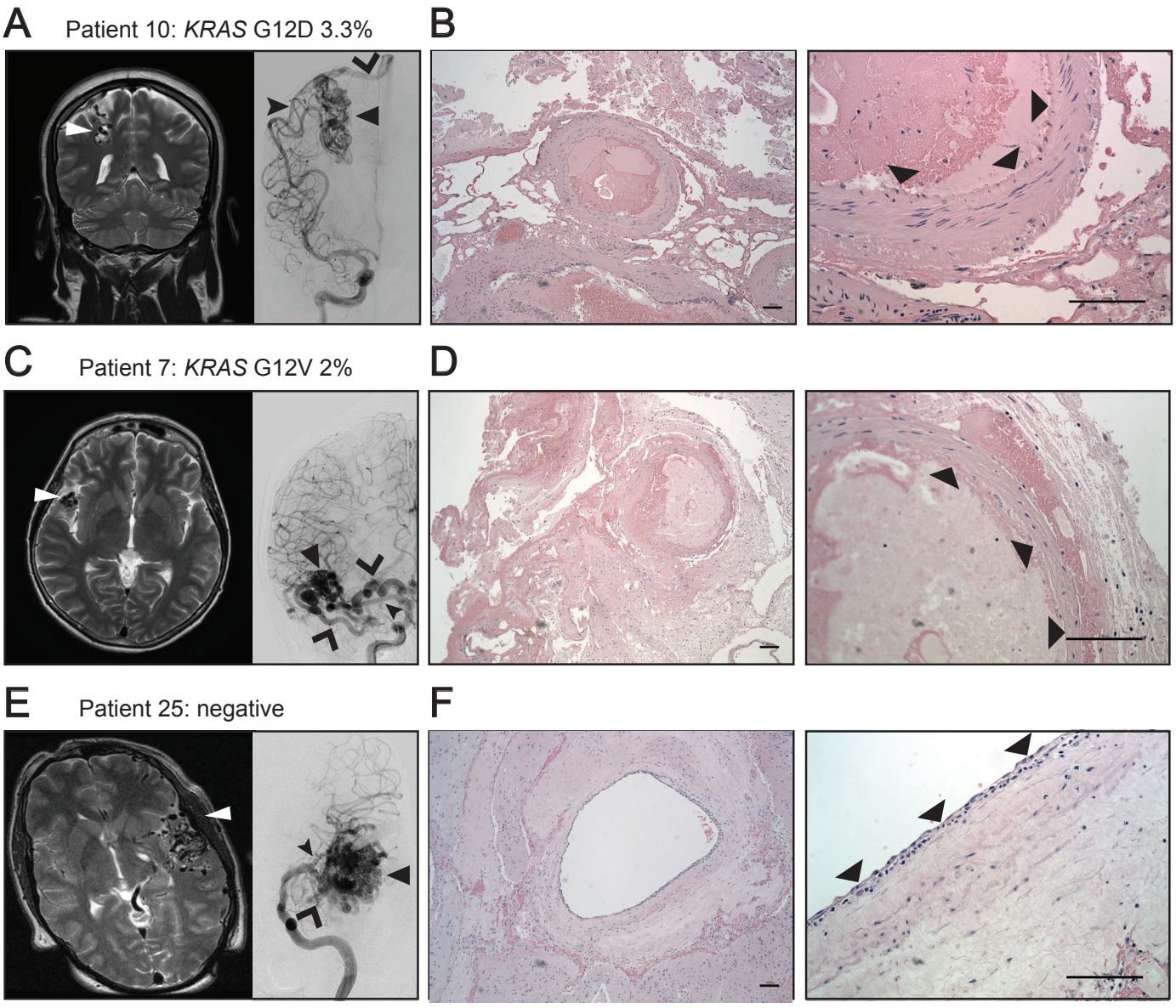

Figure S1: Examples of brain arteriovenous malformations (BAVMs) in this study. (A, C, E) Right: MRI T2 sequence (right) showing BAVMs. Characteristic dark flow voids delineate the nidus (white arrowheads) and surrounding feeding arteries and draining veins. Left: angiographic appearance of BAVMs, demonstrating BAVM angioarchitecture: feeding arteries (black arrowhead) directly connect to the nidus (black pointer) and shunt arterialized blood in early filling draining vein(s) (open arrowhead). **(B, D, F)** Histopathological appearance of BAVMs shown in A, C, and E respectively, composed of abnormal vessels of varied size and thickness. The vessel wall consists of a single endothelial cell lining and a multilayer thick wall of smooth muscle cells. Brain or loose connective tissue is found between the vessels. Left panels are magnified 10x, right panels 40X. **(A, B)** A right parietal BAVM in Patient 10 carries a *KRAS* c.35G>A;p.(Gly12Asp) variant with an abundance of 3.3% which represents 6.6% of cells in the specimen, assuming that the variant is heterozygous. **(C, D)** A right temporal BAVM in Patient 7 carries a variant in c.35G>A;p.(Gly12Asp) with an abundance of 2% (4% affected cells) and **(E, F)** A left temporal BAVM in Patient 25, which was negative for *KRAS* variants. Scale bars = 100 μm.

Patient 1
nidus

p.G12D

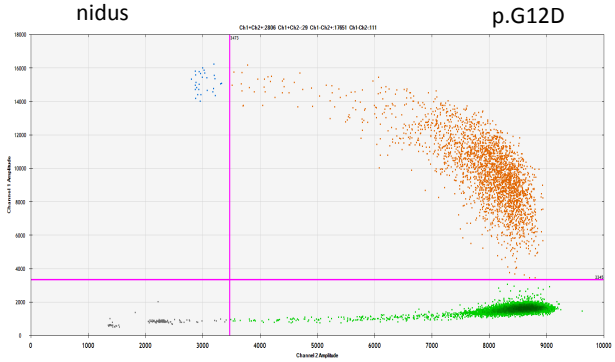

Patient 1
vein

p.G12D

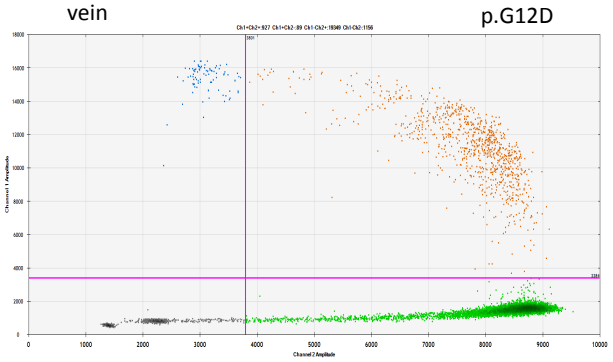

Patient 2

p.G12V

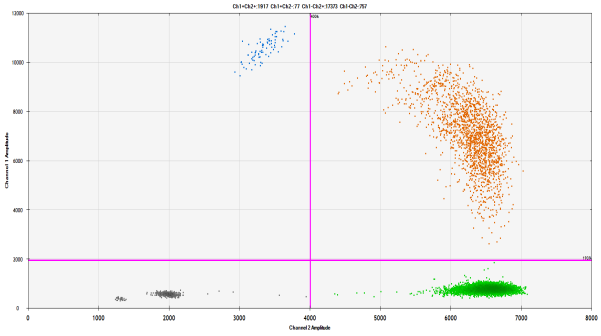

Patient 3

p.G12D

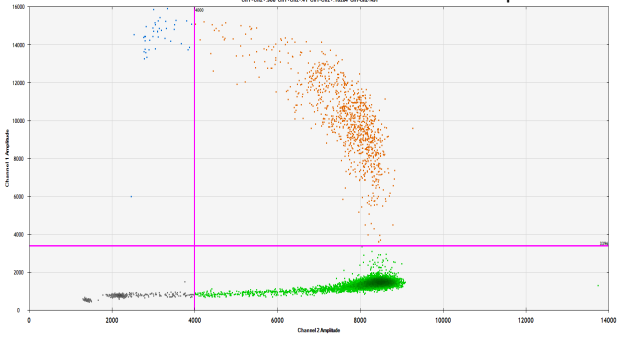

Patient 4

p.G12D

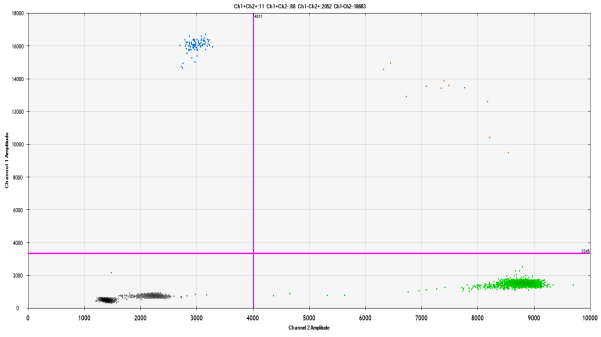

Patient 5

p.G12V

Figure S2

Patient 6 p.G12D

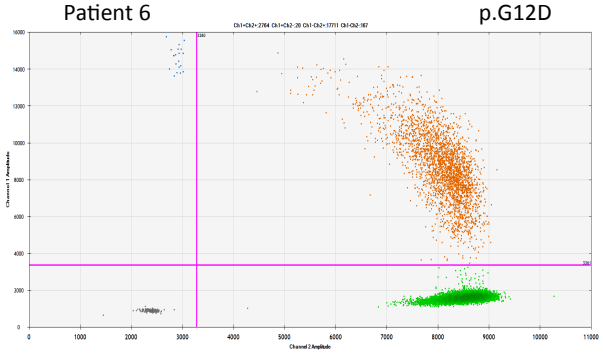

Patient 7 p.G12V

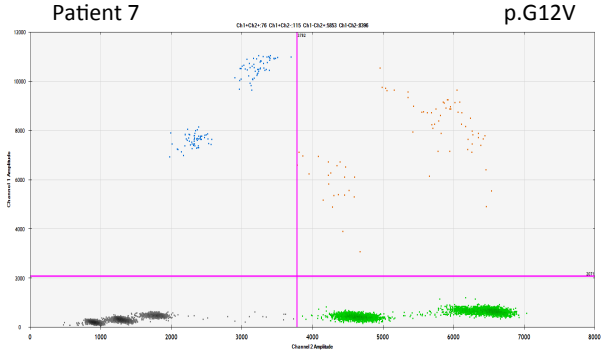

Patient 8 p.Q61H

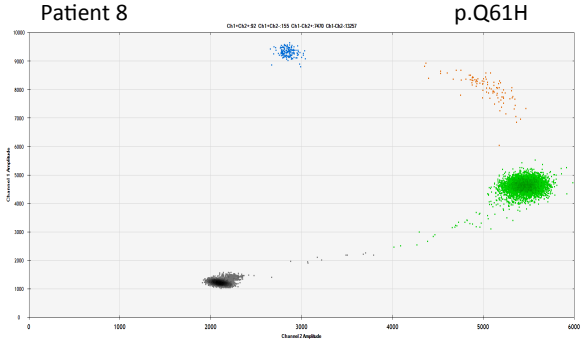

Patient 9 p.G12V

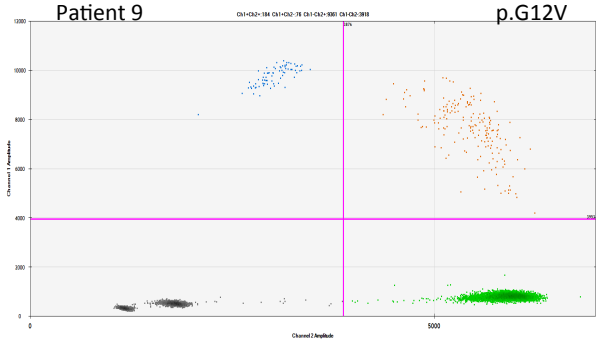

Patient 10 p.G12D

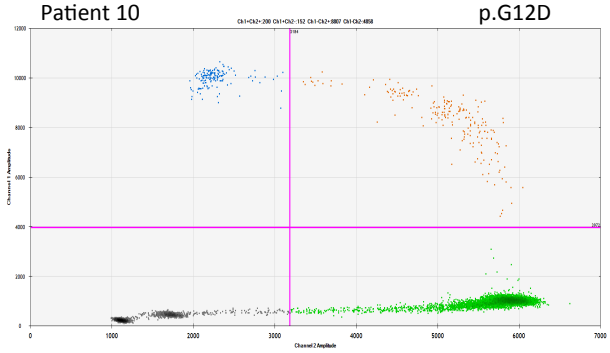

Patient 11 p.G12V

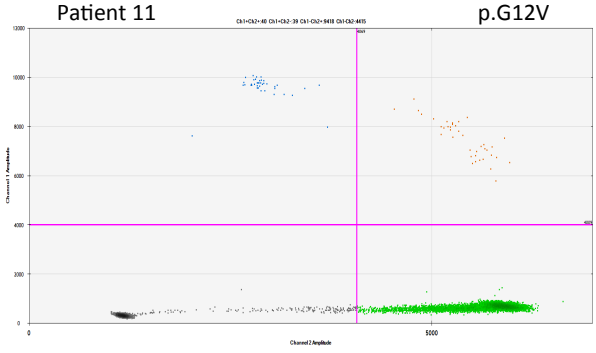

Figure S2 - continued

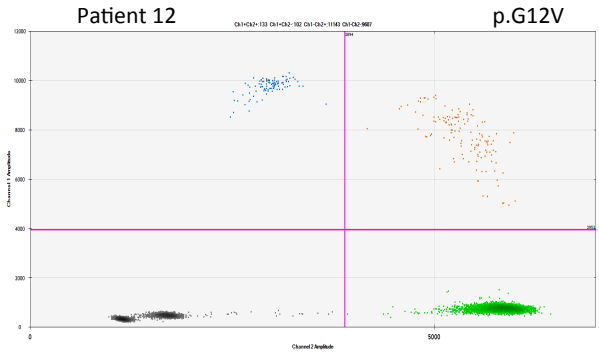

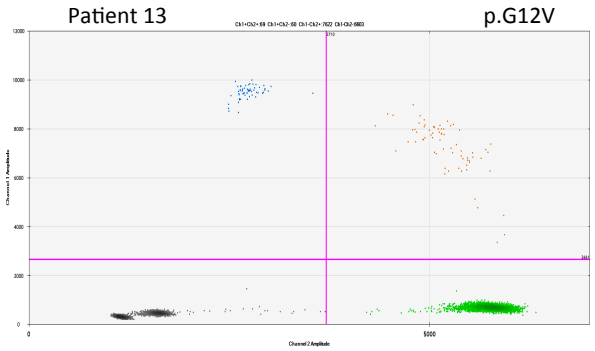

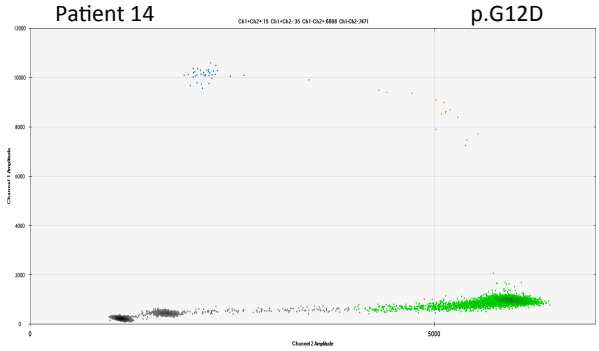

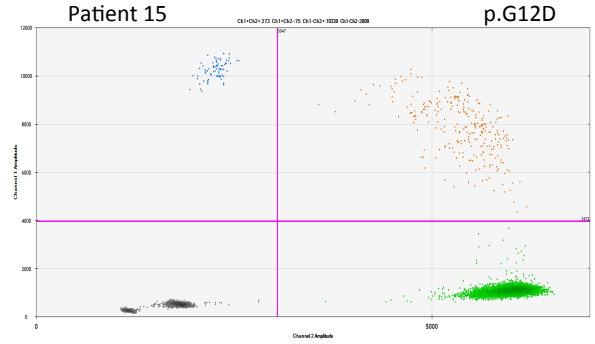

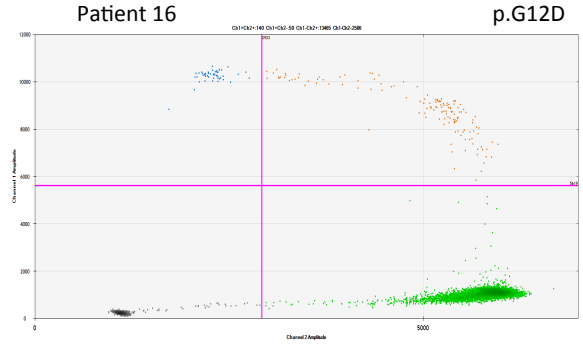

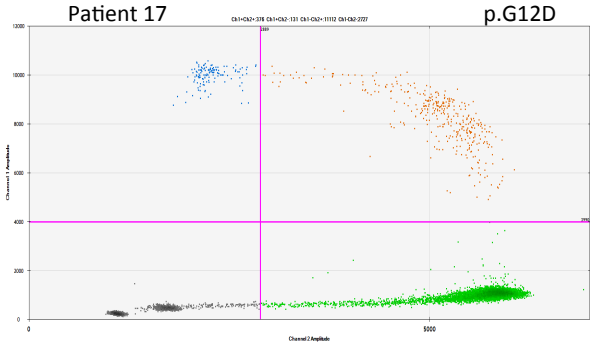

Figure S2 - continued

Patient 18 p.G12D

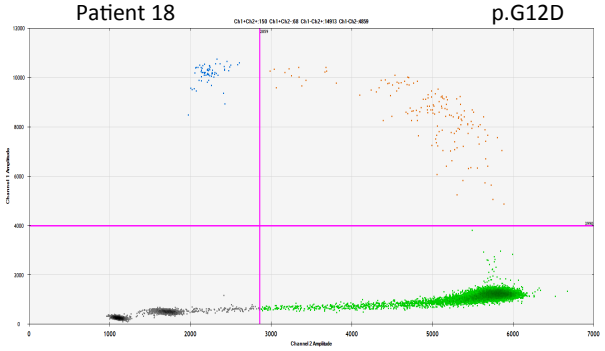

Patient 28 p.G12D

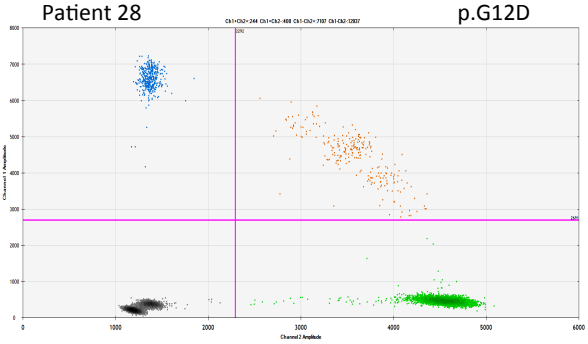

Patient 29 p.G12D

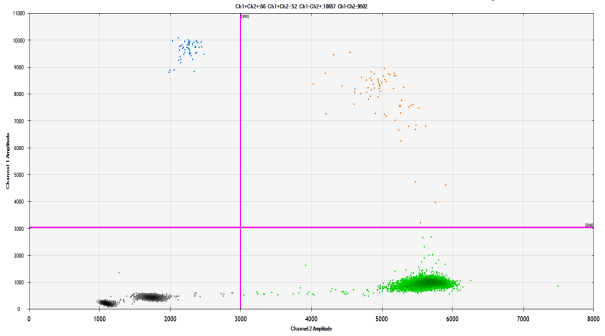

Patient 29, AVM1, EC-enriched p.G12D

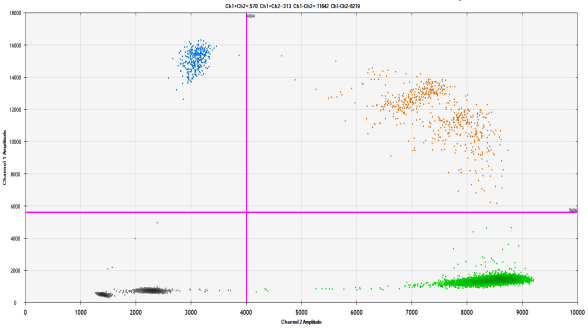

Patient 30 p.G12V

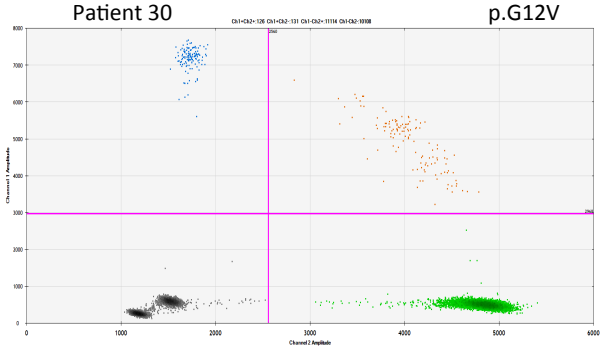

Patient 30, AVM2, EC-enriched p.G12V

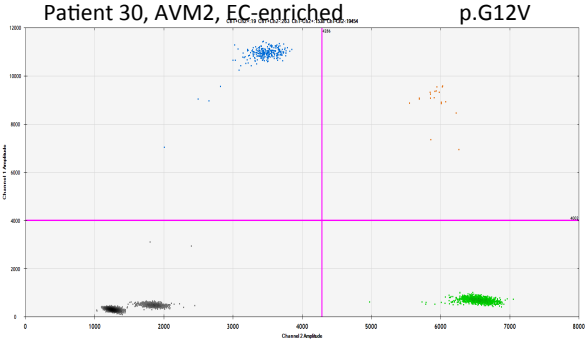

Figure S2 - continued

Patient 31 p.G12D

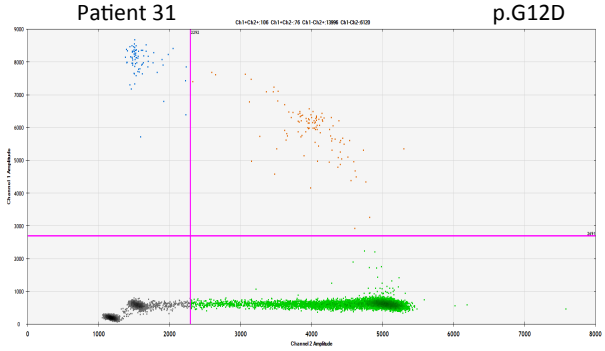

Patient 31, AVM3, EC-enriched p.G12D

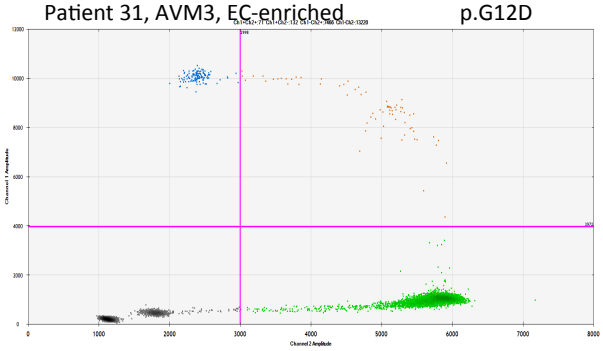

H441 – positive control p.G12V

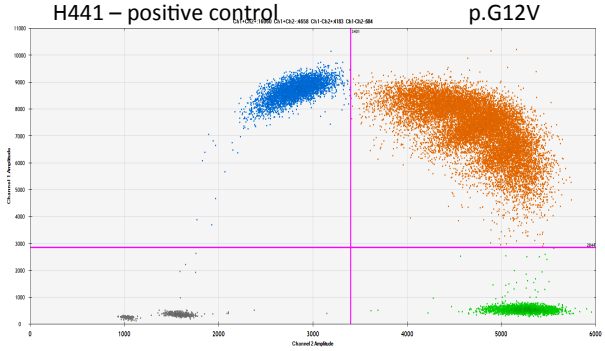

Patient 32, AVM4, EC-enriched p.G12D

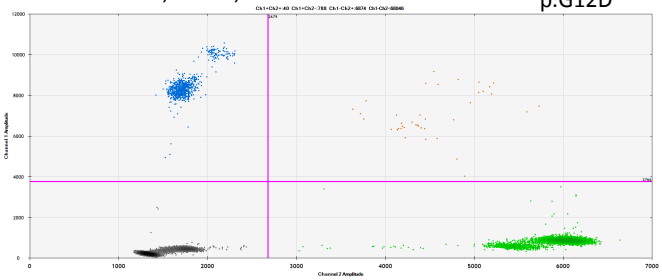

Figure S2 - continued

Patient 33 p.G12D

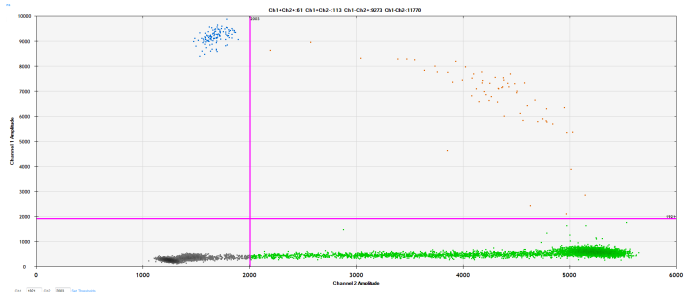

Patient 34 p.G12D

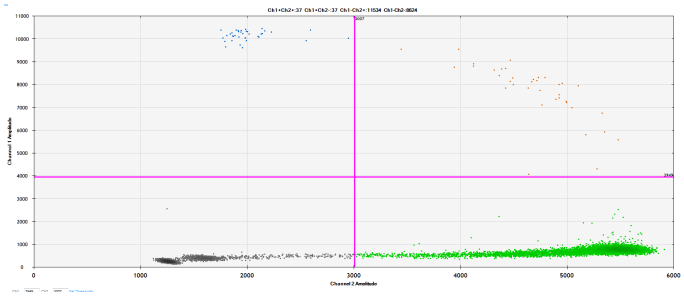

Patient 35 p.G12V

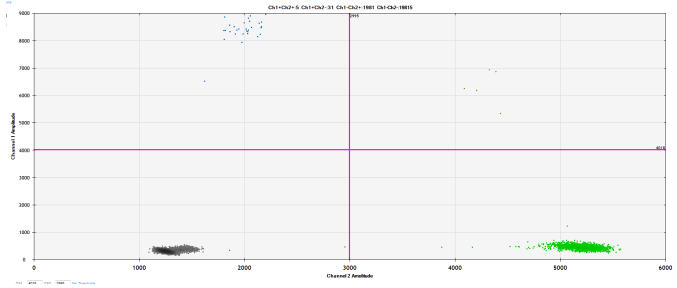

Patient 36 p.G12D

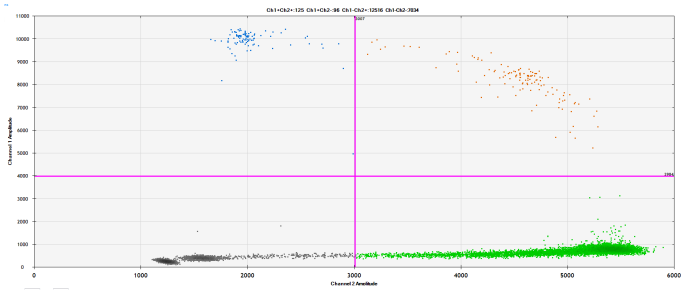

Patient 37 p.G12D

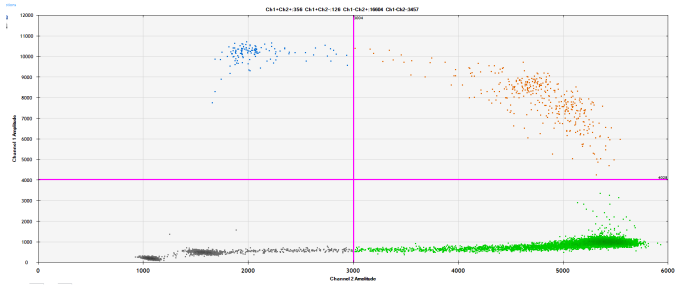

Figure S2 - continued

Patient 39 p.G12D
Nidus

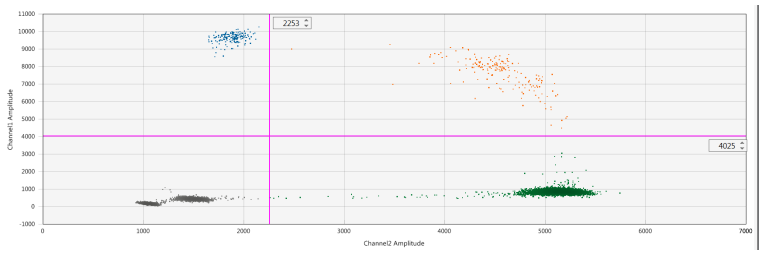

Patient 39 p.G12D
Vein

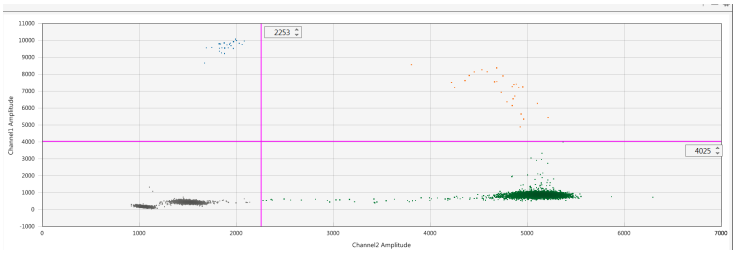

Figure S2: Amplitude scatter plots of *KRAS* c.35G>T;p.(Gly12Val) and c. 35G>A;p.(Gly12Asp) ddPCRs of frozen samples (Toronto cohort). All BAVM samples (including EC-enriched samples) with their respective anonymized patient numbers are shown. Dots represent single well data. Chanel 1 is the variant assay (FAM) duplexed with the wild-type reference assay (HEX, Chanel 2). Positive events are in the upper quadrant of each plot.

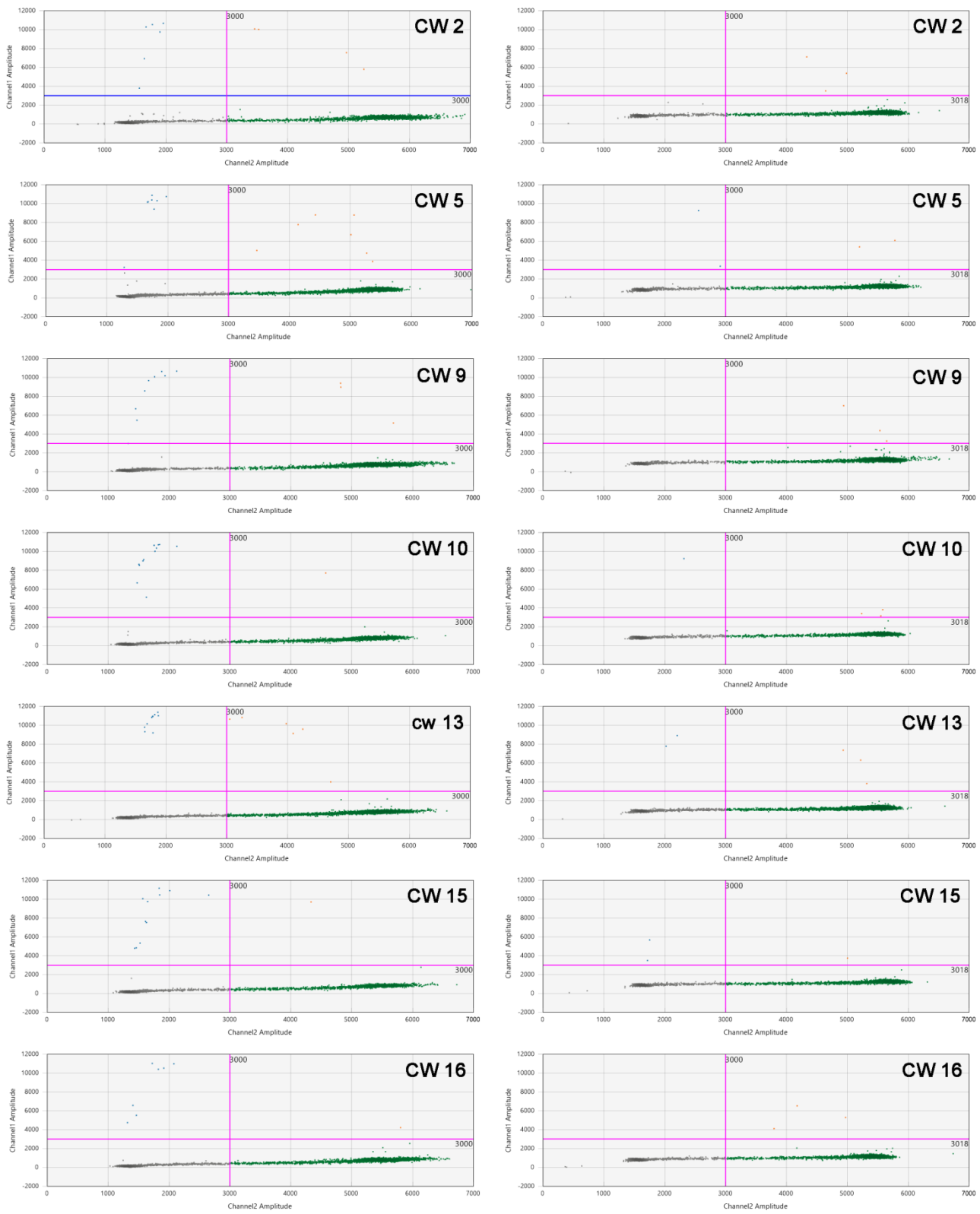
KRAS G12D, non-treated gDNA:
KRAS G12D, UDG-treated gDNA:
CW 2
CW 5
CW 9
CW 10
cw 13
CW 13
CW 15
CW 16
Channel1 Amplitude
Channel2 Amplitude
3000
3018

Figure S3

KRAS G12D, non-treated gDNA:

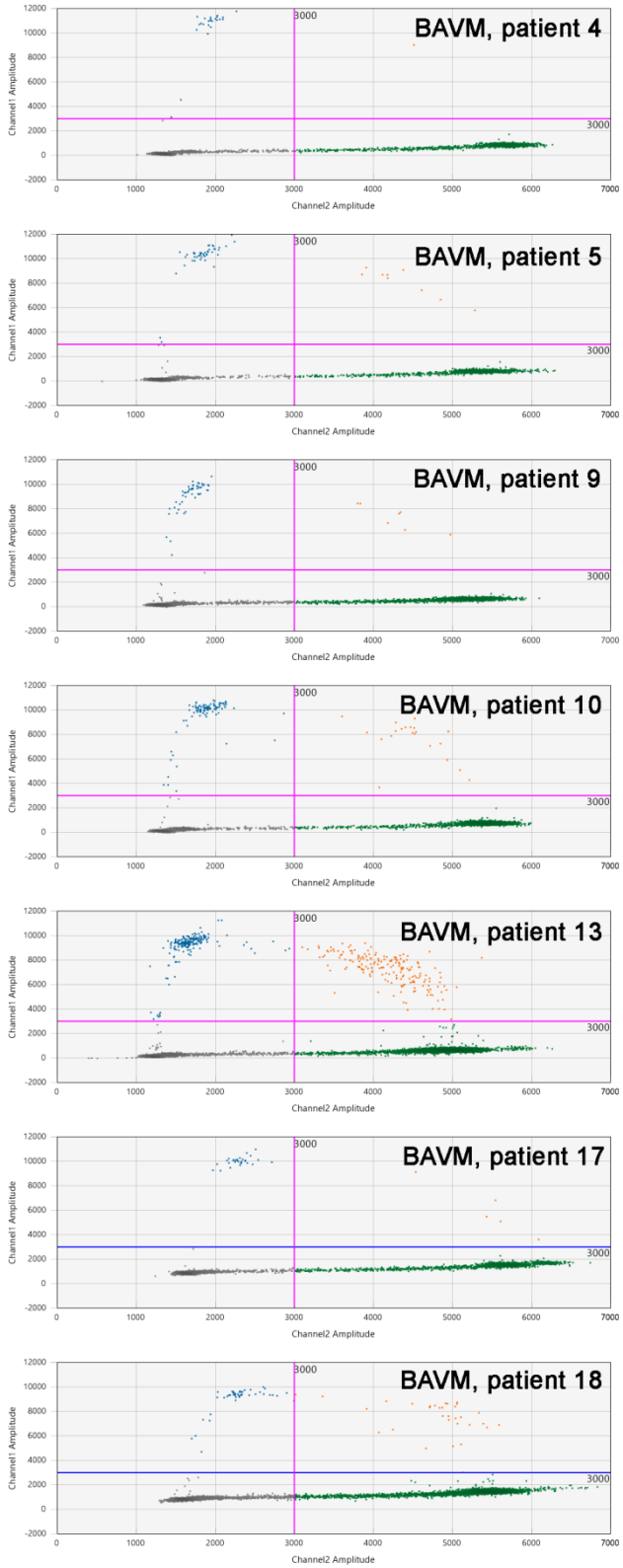

KRAS G12D, UDG-treated gDNA:

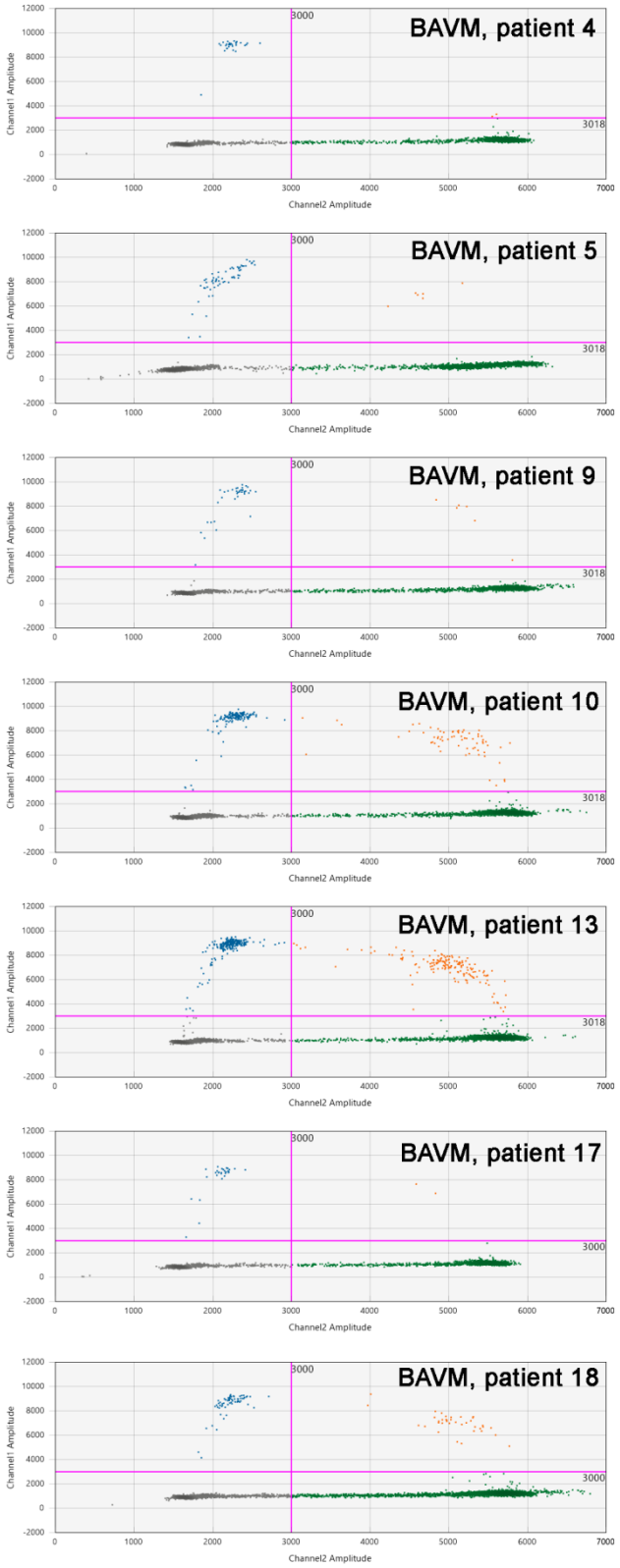

Figure S3 - continued

KRAS G12D, non-treated gDNA:

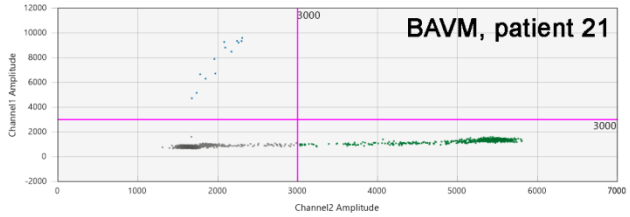

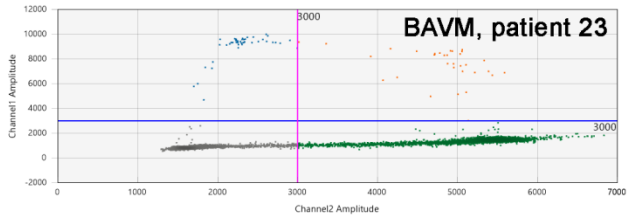

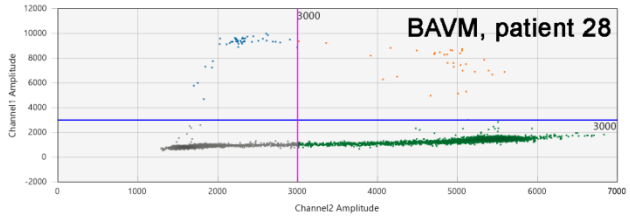

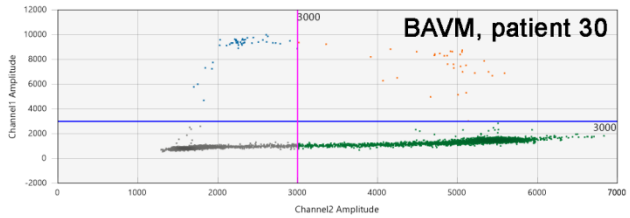

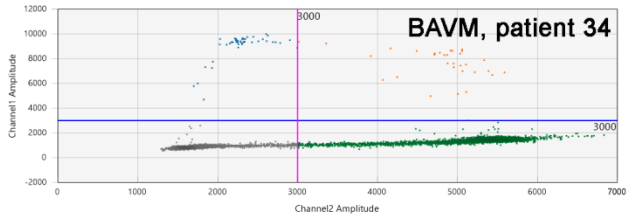

KRAS G12D, UDG-treated gDNA:

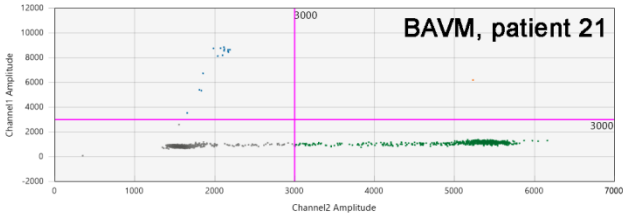

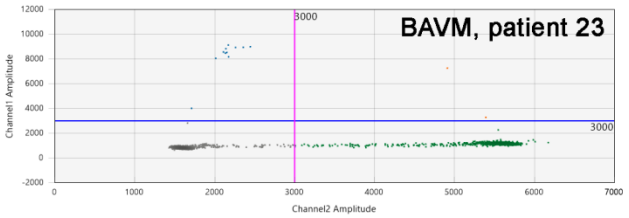

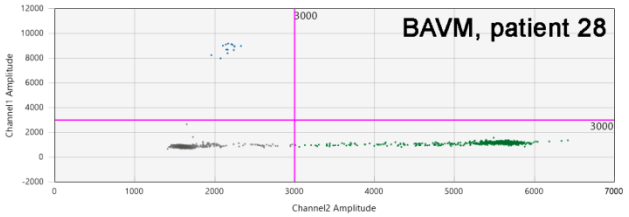

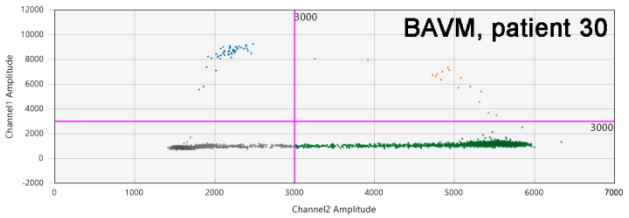

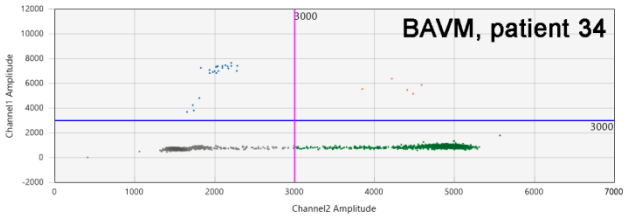

KRAS G12D, control DNA sequences:

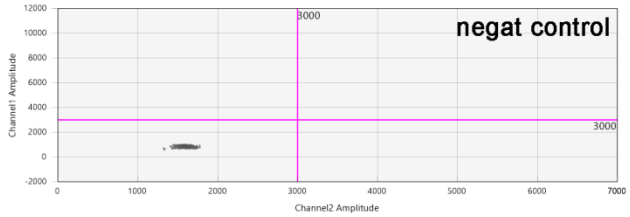

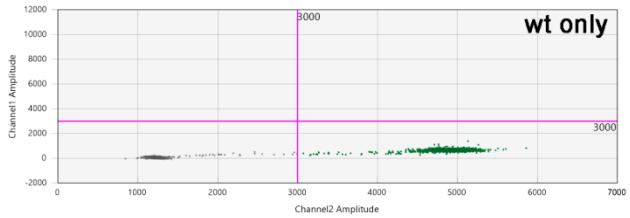

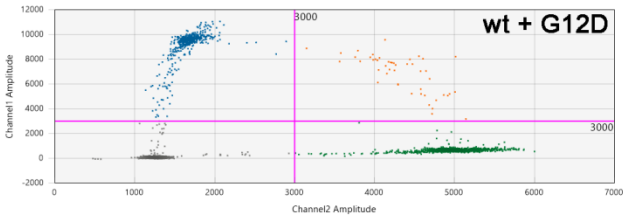

Figure S3 - continued

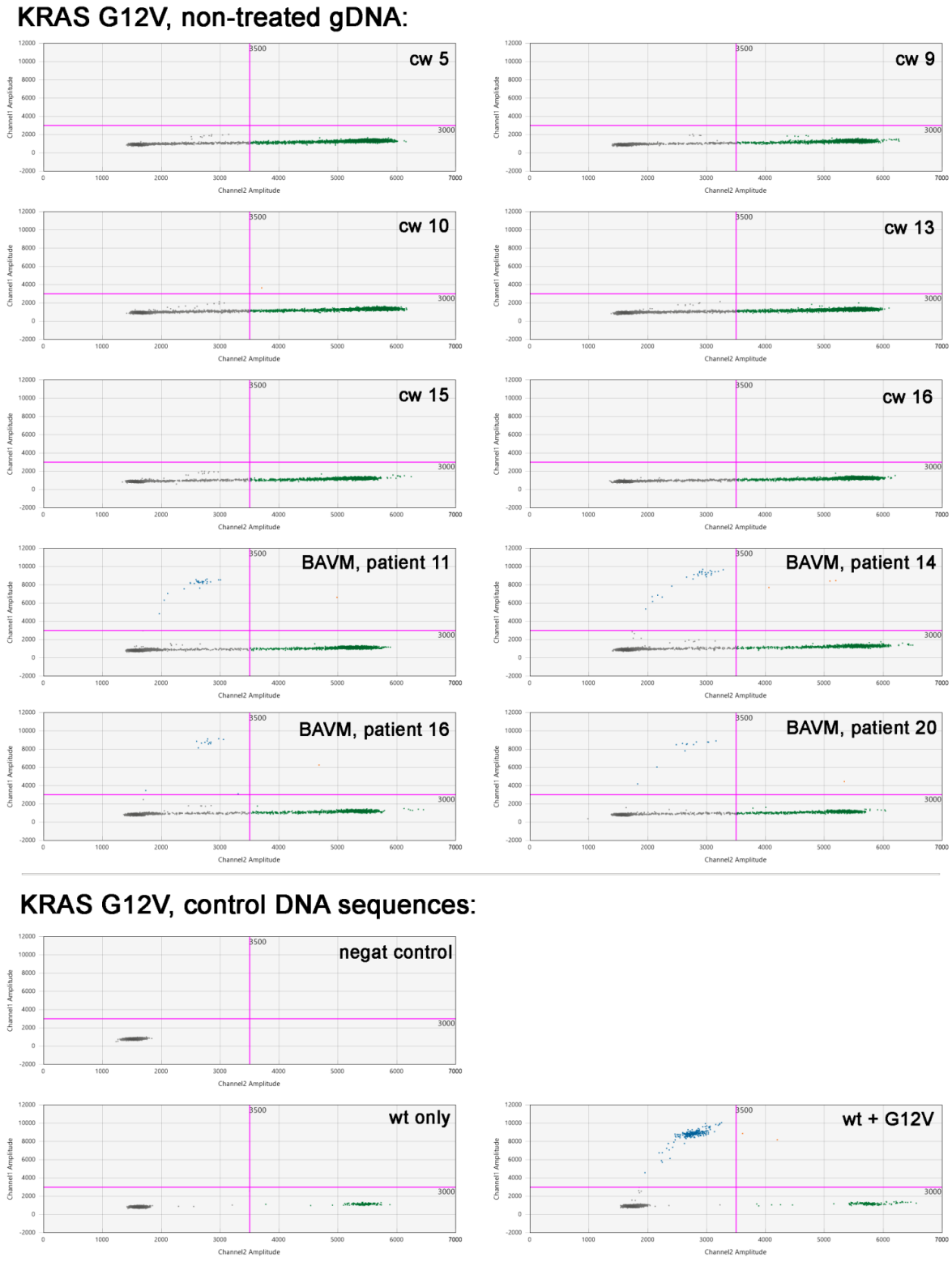

Figure S3: Amplitude scatter plots of *KRAS* c.35G>T;p.(Gly12Val) and c.35G>A;p.(Gly12Asp) ddPCRs of FFPE sample (Finnish cohort) with and without UDG treatment. ddPCR plots with and without uracil DNA glycosylase treatment for a representative subgroup of Circle of Willis control samples from the KUH cohort is shown. All variant-positive BAVM samples from the KUH cohort with their respective anonymized patient numbers are shown with and without UDG treatment. Dots represent single well data. Chanel 1 is the variant assay (FAM) duplexed with the wild-type reference assay (HEX, Chanel 2). Positive events are in the upper quadrant of each plot.

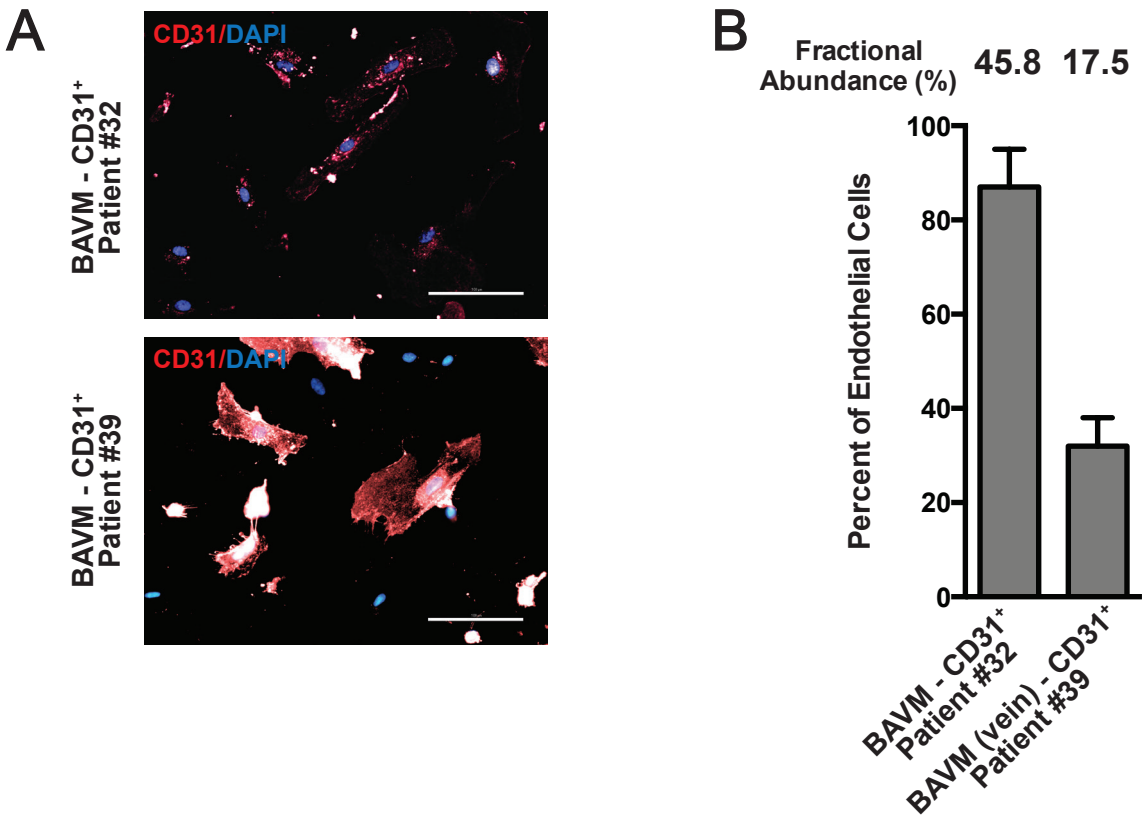

Figure S4: Endothelial cell enrichment of *KRAS* variants in BAVMs. (A) CD31 immunostaining of MACS-sorted CD31⁺ fractions of BAVMs from Patients #32 and #39 used for quantification of endothelial cells. Scale bars=100 µm. **(B)** Quantification of CD31⁺ cells in CD31 MAC-sorted fractions of BAVMs from Patients #32 and #39 compared to their respective allele frequency of *KRAS* variants.

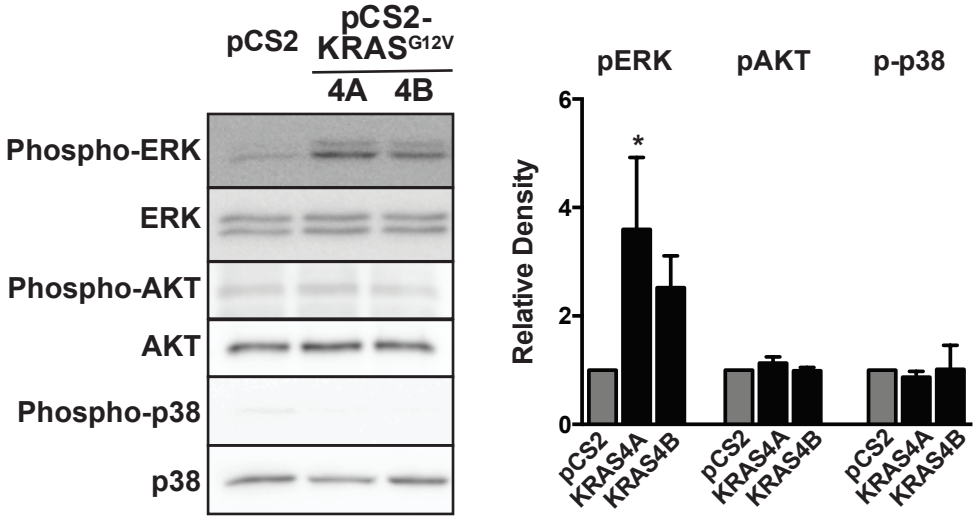

Figure S5: Active KRAS specifically induces ERK1/2 phosphorylation in endothelial cells. HUVEC expressing c.35G>T;p.(Gly12Val) KRAS isoforms 4A or 4B show elevated phospho-ERK levels, whereas no increases in phospho-Akt or phospho-p38 are detected.

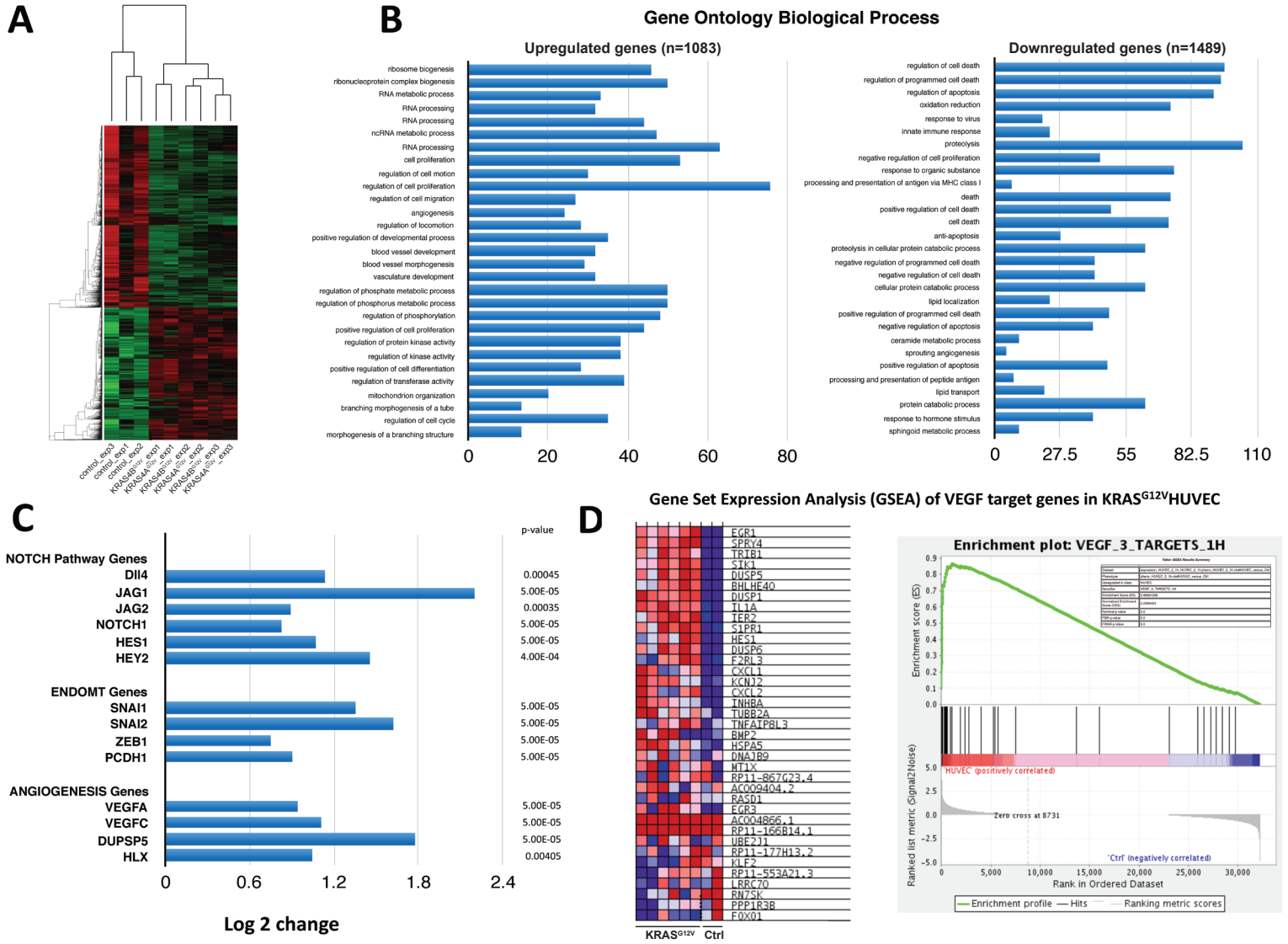

Figure S6: Expression of activated KRAS induces pro-angiogenic and Notch pathway genes in endothelial cells. (A) Heatmap showing general clustering of control Human Umbilical Endothelial Cells (HUVECs) versus KRAS4A^{G12V}- and KRAS4B^{G12V}-expressing HUVECs. **(B)** Gene Ontology (GO) term biological process analysis of upregulated and downregulated genes in KRAS^{G12V}-expressing HUVECs showing the 30 most significant biological processes. Bars show the number of genes with significant differential expression for each biological process. **(C)** Over-expression of KRAS^{G12V} induced the expression of several Notch signaling components (i.e. *DLL4, JAG1, JAG2, NOTCH1, HEY2, HES1*), Endothelial to Mesenchymal Transition (EndoMT) genes (i.e *SNAI1, SNAI2, ZEB1, PCDH1*) and induced angiogenic genes (*VEGFA, VEGFC, HLX*) and a MAPK/ERK-responsive gene (*DUSP5*). **(D)** Heatmap showing differential expression of a VEGF induced gene set in HUVECs and Gene Set Expression Analysis showing enrichment of VEGF induced genes in KRAS^{G12V}-expressing HUVECs.

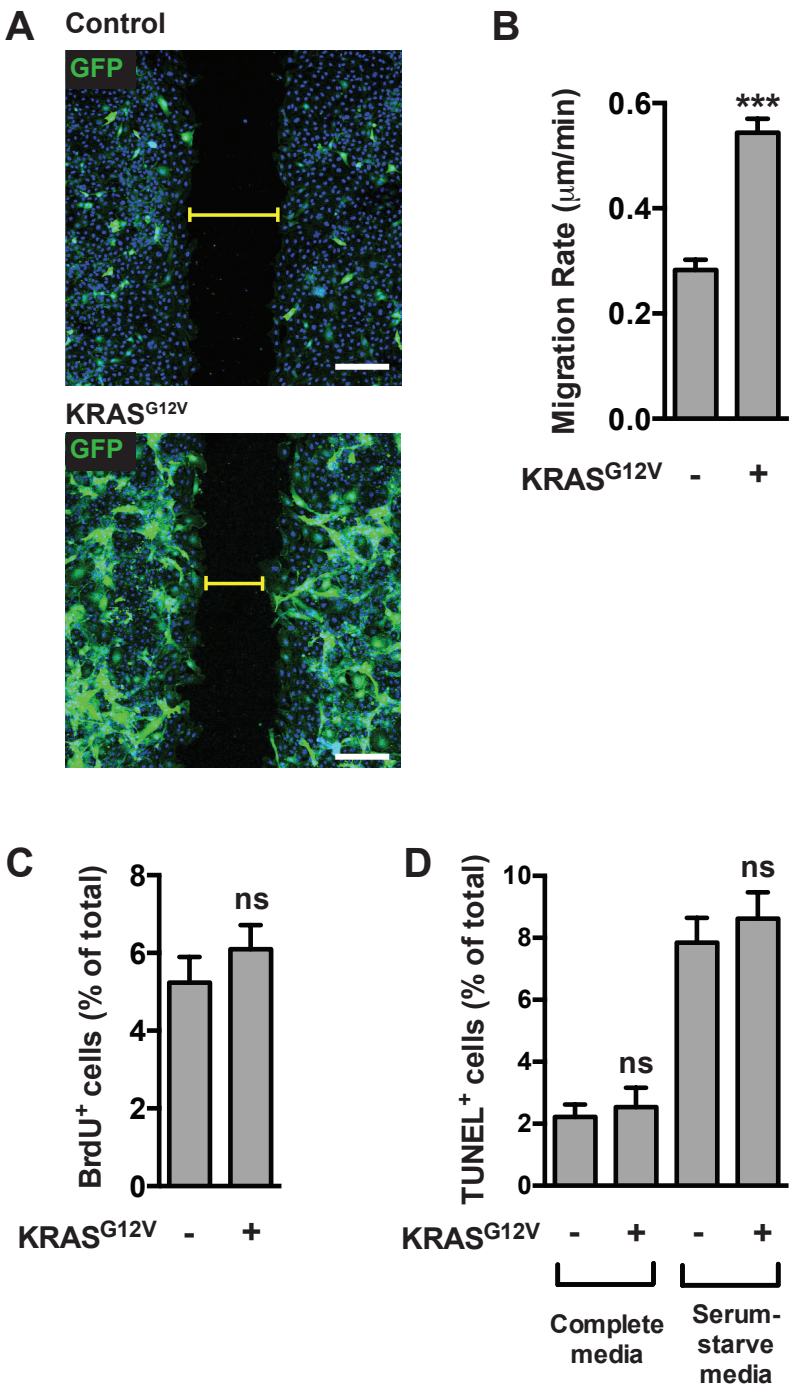

Figure S7: Expression of activated KRAS induces a pro-angiogenic phenotype in HUVECs. **(A)** Expression of KRAS4A^{G12V} resulted in altered cell morphology in an 8 h 'scratch' assay performed in the absence of growth factors or FBS. Scale bar = 200 μm. **(B)** Migration rate in serum-starve media was quantified by tracking multiple individual cells during time-lapse confocal microscopy in a 'scratch' assay. n=37 cells (from 14 videos) for control and n=41 (from 15 videos) for KRAS4A^{G12V} from a representative experiment. See Supplemental Video 1 for a representative time-lapse. **(C)** Cell proliferation in serum-starve medium was measured by BrdU incorporation. n = 23-24 non-overlapping fields of view from 3 independent experiments. **(D)** TUNEL staining in serum-starve or complete media revealed no differences in apoptosis in cells expressing KRAS4A^{G12V}. n = 17-18 fields of view from 3 independent experiments.

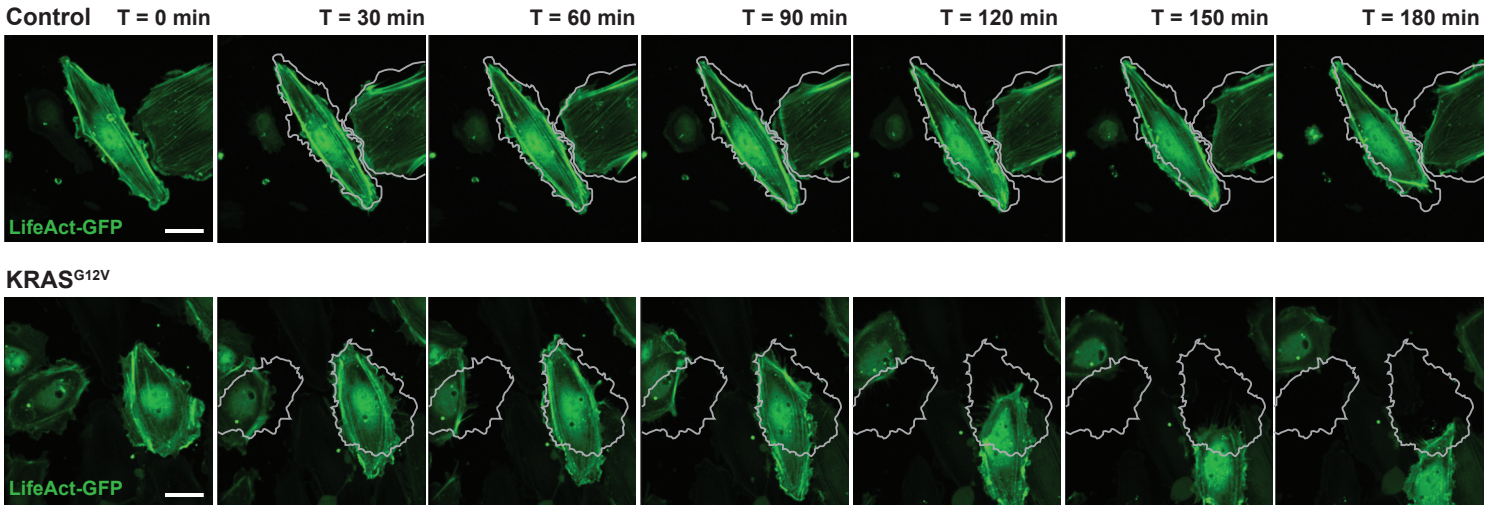

Figure S8: Expression of KRAS^{G12V} enhances migratory behaviour in a human arterial endothelial cell line (Telo-HAEC). Actin dynamics (LifeAct-GFP) were altered upon expression of KRAS4A^{G12V} in the absence of a migratory cue. Actin turnover was more rapid and cells displayed increased motility (an outline of the position of the cells at the beginning of the time-lapse is indicated). Static images from representative videos (Supplemental Video 3) are shown. Scale bar = 20 μm.